Handbook of Star Forming Regions Vol. I
Astronomical Society of the Pacific, 2008
Bo Reipurth, ed.

The Perseus Cloud

John Bally

Center for Astrophysics and Space Astronomy, University of Colorado, 389 UCB, Boulder, CO 80389, USA

Josh Walawender

Institute for Astronomy, University of Hawaii, 640 N. Aohoku Pl., Hilo, HI 96720, USA

Doug Johnstone, Helen Kirk

National Research Council of Canada, Herzberg Institute for Astrophysics 5071 W. Saanich Rd., Victoria ON V9E 2E7, Canada

Alyssa Goodman

Harvard-Smithsonian Center for Astrophysics 60 Garden Street, Cambridge, MA 02138, USA

Abstract. The Perseus molecular cloud and its surroundings contain several regions of active or recent star formation lying within about 300 pc of the Sun (see Figure 1). Roughly a dozen OB and over a thousand lower mass stars younger than 6 Myr make up the 50 pc diameter Perseus OB 2 association. Recent supernovae in the Per OB2 association drive an expanding HI supershell into the surrounding interstellar medium. A run-away star from this association, ξ Persi, illuminates and ionizes a portion of this ring, producing the California Nebula (NGC 1499, Sh-2 220). The 10^4 $M_{\odot}$ Perseus molecular cloud is the closest such object actively forming large numbers of low to intermediate-mass stars. The eastern end of the cloud is associated with the 2 – 4 Myr old cluster IC 348 that contains several hundred young stars. However, the western portion of the Perseus cloud contains the most active sites of current star formation, including the 150 member NGC 1333 cluster, the small stellar aggregates associated with Barnard 1, L1448, L1455, and additional cloud cores which are producing smaller groups of young stars. Narrow-band visual wavelength surveys have led to the discovery of over a hundred individual Herbig-Haro objects. Studies of outflows in the Perseus molecular cloud have illuminated their contribution to the generation of turbulent motions in the surrounding gas, the disruption of cloud cores, and the self regulation of star formation. In this review, we cover the region of the sky from about l = 150° to 180° and $b = -30°$ to 0°, and the young stars, clusters, and clouds which lie between 200 and 400 pc from the Sun with ages of less than about 15 Myr with an emphasis on the Perseus molecular cloud. This is the sphere of influence of the Per OB2 association. We discuss the 20° diameter Per OB2 supershell, the OB association, its relationship to surrounding molecular gas, and on-going star formation within the Perseus molecular cloud.

1. Introduction

We start this review with a discussion of the Per OB2 association (Section 2) and its relationship to the Gould's Belt and Lindblad ring of young stars and gas in the solar vicinity. We then discuss the properties of the interstellar medium towards Per OB2, and its relationship to the Perseus molecular cloud (Section 3), the most active region of star formation within 300 pc of the Sun (Ungerechts & Thaddeus 1987; Sun et al. 2006). Next, we discuss the results of large-scale surveys of molecular gas and dust, Herbig-Haro objects, outflows, and stellar populations within Perseus (Hatchell et al. 2005; Walawender et al. 2005a; Kirk, Johnstone, & Di Francesco 2006; Jørgensen et al. 2006, 2007). Lastly, we discuss individual regions such as Barnard 5, IC 348, Barnard 1, NGC 1333, L1455, L1448, and several other less well known portions of the Perseus complex in detail (Section 4).

The sphere of influence of the Per OB2 association extends from about $l = 150°$ to $180°$ and $b = -30°$ to $0°$. It contains young stars, clusters, and clouds which lie between 200 and 400 pc from the Sun with ages of less than about 15 Myr. Figure 1 shows an overview of the Perseus region.

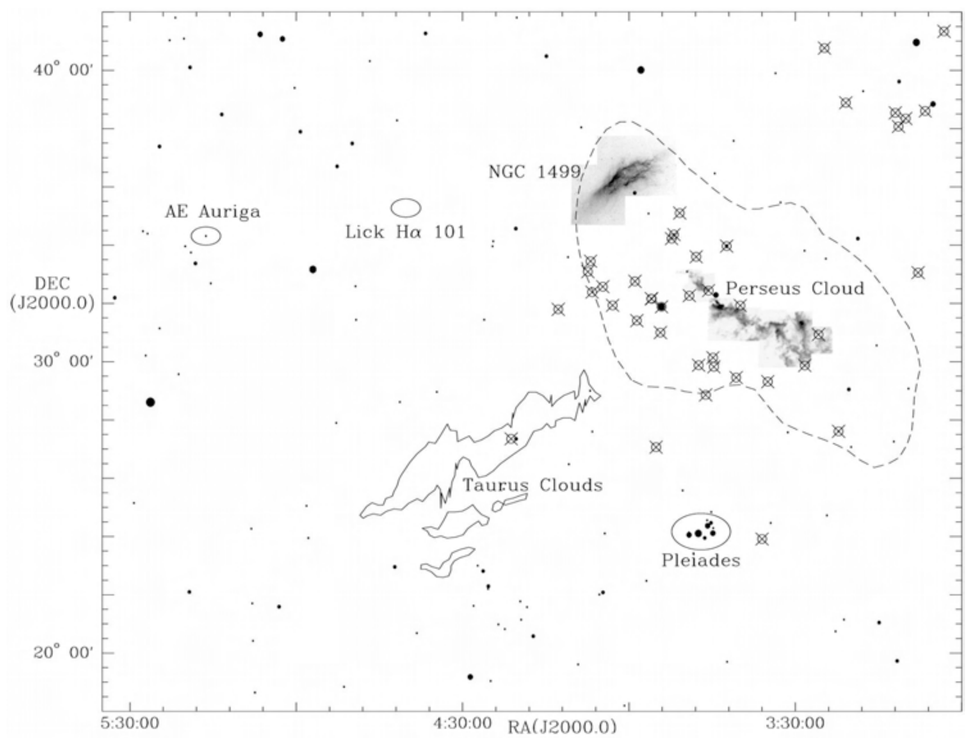

Figure 1. Overview of the Perseus region showing the locations of the brightest Per OB2 stars (circles combined with crosses), the outline of the HI supershell (dashed outline on the right side of the figure), and the molecular cloud (grey-scale inset inside the dashed outline) which is shown in greater detail in Figures 2 and 3. The HII region NGC 1499 (the California Nebula) that is illuminated by the run-away star ξ Per (a member of Per OB2) is shown in grey-scale on the northeast side of the supershell. The Pleiades, the Taurus molecular clouds, the run-away star AE Aurigae, and the background star forming region LkHα 101 are also indicated.

2. The First Generation: The Perseus OB2 Association

The Per OB2 association is the second closest OB association to the Sun with an age less than 15 Myr (Blaauw 1952; Borgman & Blaauw 1964; Blaauw 1964 – the Sco-Cen OB association, located between 100 to 200 pc from the Sun in the fourth and first quadrants of the Milky Way, is the nearest such group; see chapter by Preibisch & Mamajec). Although not as rich or as well endowed with massive stars, Per OB2 is nevertheless one of the major OB associations in the Solar vicinity (e.g. Blaauw 1991).

The Per OB2 association is about 6 Myr old (de Zeeuw et al. 1999) and may have formed from the far-side of the Lindblad Ring of HI associated with the Gould's Belt of B and A stars (Olano & Poppel 1987). In this picture, an expanding supershell, possibly triggered by the 50 to 90 Myr-old Cas-Tau 'fossil' OB association centered in the general vicinity of the α Persei cluster ([l, b] = [146°, -6°], d $\approx$ 180 pc, age 50 to 90 Myr; Blaauw 1991; Stauffer et al. 1999; Lodieu et al. 2005) swept up surrounding interstellar gas, decelerated it, and fragmented it into about a dozen 10^4 to 10^6 $M_\odot$ clouds within the last 20 Myrs by means of gravitational instabilities (McCray & Kafatos 1987). Subsequently, these new-formed clouds became the sites of star formation that led to the birth of the Sco-Cen, Per OB2, and Orion OB1 associations (Bally 2001).

de Zeeuw et al. (1999), using Hipparcos positions, proper motions, and parallaxes, found 41 members of Per OB2, most of which have spectral type B and A. The most massive main sequence member is the B0.5V star 40 Per. However, the Hipparcos members provide a severe lower-bound to the population in Per OB2. Belikov et al. (2002) identified over 800 members in a roughly 50 pc diameter region with masses between 1 and 17 $M_\odot$ by their common proper motions and distances. Extrapolating these counts and assuming a Salpeter IMF to 0.1 $M_\odot$ implies that the Per OB2 association may have as many as 2×10^4 members.

Per OB2 has several stars more massive than 40 Per which have evolved off the main-sequence. The B1Iab supergiant ζ Per, is located near the center of the Per OB2 association. The O7IIIe star ξ Per, a run-away star, may have been expelled from the core of Per OB2 by a supernova explosion of an even more massive companion. This high-velocity star is currently illuminating the California Nebula (NGC 1499), the brightest HII region in Perseus (Figure 1). This HII region is associated with a large and complex molecular cloud (Herbertz, Ungerechts, & Winnewisser 1991). However, little or no star formation is currently associated with this HII region. The Per OB2 association also includes a high-mass X-ray binary, X Per.

Interestingly, there is a roughly 5 – 10 km s^{-1} difference between the radial velocity of the Per OB2 association and the Perseus molecular cloud. The radial velocity of the association (heliocentric) is about $V_{hel} \sim$ 23.5 km s^{-1} (Steenbrugge et al. 2003) while the cloud has $V_{hel} \sim$ 15 – 20 km s^{-1}. This velocity difference fits the scenario in which Per OB2 formed from a portion of the expanding Lindblad ring. The first-to-form older stars (Per OB2) would have a larger radial velocity than younger stars produced from gas which has been decelerated by interaction with the ISM. The radial velocity of Per OB2 indicates that when it formed about 6 Myr ago, it was about 50 to 80 pc closer, or about 100 pc from the center of expansion of the Gould's Belt / Lindblad ring.

2.1. The Atomic Hydrogen Supershell

The Per OB2 association has blown a 100 pc diameter (20°) shell of atomic hydrogen into the surrounding interstellar medium (Sancisi et al. 1974; Heiles 1984; Hartmann

& Burton 1997). Sancisi et al. (1974) noted excess HI emission associated with the Perseus molecular cloud as traced by OH emission and estimated the HI mass associated to be about M(H) = 2×10^3 M$_\odot$. Sancisi et al. also noted the kinematic signature of an expanding shell centered on the Per OB2 association. This feature is clearly seen in the Hartmann & Burton (1997) 21 cm HI atlas between V_{LSR} = -6 and +6 km s^{-1} where it is seen as a roughly 15° diameter cavity centered close to ζ Per. A series of concentric partial shells of 21 cm emission delineate the walls of this cavity. The Perseus molecular cloud appears to be embedded in the western rim of the shell. Confusion with background Galactic HI emission makes it difficult to determine a shell expansion velocity. In the Hartmann & Burton (1997) atlas, the cavity can be traced over a roughly 20 km s^{-1} velocity range; the filamentary shell walls become confused with unrelated emission beyond this region. Thus, a very rough estimate of the shell expansion speed is 10 km s^{-1}. However, there are no reliable estimates for the mass of this superbubble in the literature.

The Per OB2 supershell can be clearly seen in the long-wavelength sub-mm and far-IR maps produced by DIRBE on the COBE satellite (see Figure 1 in Watson et al. 2005). These images show a ring of dust emission surrounding a cavity centered on the Per OB2 association. They also clearly show free-free emission from the California Nebula (NGC 1499) and the faint low-surface brightness HII region, G159.6-18.5 which is superimposed on the Perseus molecular cloud.

An order-of-magnitude estimate of shell mass as traced by 21 cm emission can be made by comparison with the larger and more massive supershells associated with Orion and Sco-Cen, each of which contain a mass of about $1 - 2 \times 10^5$ M$_\odot$. The physical size of the Per OB2 shell is about 3 times smaller than either Orion's Cloak, or the Sco-Cen supershell (Heiles 1984). Scaling the mass of these shells with projected area implies a mass for the Per OB2 shell of order $1 - 2 \times 10^4$ M$_\odot$. Using the Heiles relationship between shell size and mass, $M \approx 8.5\, r_{pc}^2$ M$_\odot$ where r_{pc} is the shell radius in parsecs, r_{pc} = 50 pc, implies $M \approx 2 \times 10^4$ M$_\odot$. Thus, the kinetic energy of the shell is of order $1 - 2 \times 10^{49}$ ergs and its momentum content is about 10^5 M$_\odot$ km s^{-1}. It is likely that the shell was created by the combined effects of ionizing radiation, winds, and supernovae, that formed a hot superbubble containing shock-heated plasma. The expansion of the bubble has swept up the surrounding low-density cold and warm atomic hydrogen into the HI supershell.

2.2. Dust and Molecular Gas in the Perseus OB2 Association

Ungerechts & Thaddeus (1987) surveyed the CO emission in the Taurus, Auriga, and Perseus region. There are multiple layers of molecular gas at different distances along this line-of-sight. Portions of the Taurus/Auriga clouds, located between 120 and 200 pc from the Sun, are observed in the foreground. The most distant parts of the Taurus molecular cloud complex may be interacting with a supershell blown by the Per OB2 association (Olano & Poppel 1987). In this picture, the far side of the Taurus clouds may be on the front edge of the shell powered by Per OB2. A background layer associated with the young cluster NGC 1579 which contains LkHα101 and the HII region Sh2-222, is located at a distance of about 700 pc in the background (Herbig et al. 2004).

Several cloud components are located at approximately 300 pc and are associated with the Perseus OB2 association but, see below for a more detailed discussion of distances. The most massive of these is the Perseus molecular cloud. The clouds associated with the California Nebula are also interacting with the OB association, but not currently forming stars. Clouds located 5° north of the California Nebula and the CO cloud near the older, background open cluster NGC 1342 may also trace outlying portions of dense molecular gas associated with the Perseus complex.

2.3. The G159.6-18.5 HII Region

The IRAS 60 and 100 μm images of the Perseus region show a prominent dust ring with a radius of 0.6° centered on the star HD 278942 (= HIP 17113; de Zeeuw et al. 1999; Ridge et al. 2006a) which lies near the edge of the Perseus molecular cloud. The spectral type of this star has been uncertain. While de Zeeuw et al. (1999) and SIMBAD list the spectral type as B5, Steenbrugge et al. (2003) gives the type as B3III based on an earlier paper by Černis (1993). Andersson et al. (2000) argue it has a spectral type B0.5 – O9.5 V, making it the most massive main-sequence member of Per OB2. Andersson et al. present radio and IR images and new spectra of the central star, demonstrating that the dust ring contains a low-surface brightness HII region with a central star of earlier spectral type than previously thought. The spectral-type discrepancy may be due to the use of photometry-based color index in the presence of heavy foreground extinction. Thus, the star is probably located behind the veil of dust associated with the Perseus molecular cloud. An HII region is clearly confined by the ring of dust and appears to lie behind the obscuration of the Perseus molecular cloud. Figure 2 shows a low angular-resolution Hα image of the G159.6-18.5 HII region superimposed on the 2MASS/NICER extinction map of the Perseus molecular cloud.

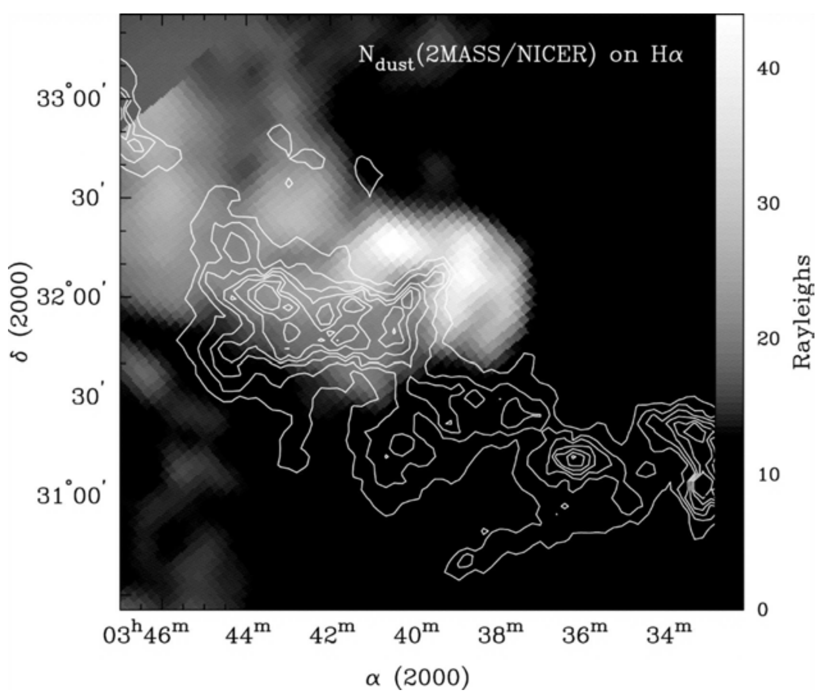

Figure 2. An Hα image of G159.6-18.5 from Finkbeiner (2003) overlaid on extinction contours derived from 2MASS/NICER (from Ridge et al. 2006a). The Hα image shows the 1.2° diameter diffuse HII region G159.6-18.5 located behind the Perseus molecular cloud and ionized by the O9.5 / B0.5 star HD 278942.

The radial velocity of HD 278942 is V_{hel} = 32 km s^{-1} (V_{LSR} = 28 km s^{-1}), about 18 km s^{-1} higher than the Perseus molecular cloud, and about 8 km s^{-1} higher than the Per OB2 association (the mean heliocentric velocity of Per OB2 is V_{hel} = 23.5 km s^{-1}; Steenbrugge et al. 2003). Thus, this star is likely to be an additional run-away from Per OB2. A lower bound on the age of this star can be estimated by assuming that it originated in the Perseus molecular cloud and that it was subsequently ejected by a dynamical interaction, possibly in the IC 348 cluster. If the separation between the current location of the star and its point of origin is comparable to the radius of the HII region, then the age of the star is $\tau > r_{HII}/V_* \sim 5\times10^5$ years where we used the radial velocity difference between the CO cloud and the star as an estimator of V_*. A young age is consistent with the observed presence of hot dust and circumstellar material in the immediate vicinity. The presence of HD 278942 and its HII region suggests that that massive stars may have formed in the recent past within the Perseus molecular cloud.

Watson et al. (2005) analyze the sub-millimeter to centimeter wavelength spectrum of G159.6-18.5 and show that between 11 and 17 GHz this ring exhibits a bump of excess emission which can not be explained as free-free emission from a plasma or thermal radiation produced by grains. They interpret this excess cm-wave emission as electric dipole, and possibly magnetic dipole radiation produced by spinning dust grains. Thus, the dust in this portion of the Perseus complex is one of the first regions to exhibit the emission mechanism proposed by Draine & Lazarian (1998; 1999).

3. The New Generation: The Perseus Molecular Cloud

The Perseus molecular cloud is the most active site of on-going star formation in the Perseus OB2 association. In the following, we first review the global properties of the Perseus cloud, then discuss the individual star forming regions in the cloud (Section 4.).

The dark clouds in Perseus were first noted by Barnard (1913; 1919) on his long time-exposure photographs. Barnard catalogued the dark clouds in this region as Barnard 1-5 and Barnard 202-206. Figures 3 and 4 show visual-wavelength images of the eastern and western portions of the Perseus dark clouds. Since the first HI and OH survey of Sancisi et al. (1974), the Perseus region has received increasing attention. Early CO observations (Sargent 1979) revealed a molecular cloud with a large velocity gradient. Low resolution (9 arcminute beam) surveys were conducted with the Columbia / CfA millimeter telescope (Ungerechts & Thaddeus 1987; Dame et al. 1997; Dame et al. 2001). Higher resolution J = 1-0 CO maps (1.7$'$ beam) were obtained with the Bell Labs 7 meter radio telescope in the mid-1980s but not published until 1994 (see Miesch & Bally 1994; Figures 5 and 6) and more recently with the Five College Radio Astronomy Observatory (FCRAO) 14 meter radio telescope as part of the COMPLETE project (Ridge et al. 2006b). Star counts were used in the mid-1980s to map the extinction in the Perseus cloud and to estimate its mass independent of the radio surveys (Bachiller & Cernicharo 1986a,b). A newly derived extinction map has been produced (Ridge et al. 2006b) using images from the Two Micron All Sky Survey (2MASS) and the Near-Infrared Color Excess Revisited (NICER) technique (Lombardi & Alves 2001).

In recent years the entire Perseus cloud has been mapped in dust continuum at 850 μm with the Sub-millimeter Common User Bolometer Array (SCUBA) on the 15 meter James Clerk Maxwell Telescope (Hatchell et al. 2005; Kirk et al. 2006) and at 1.1 mm with Bolocam on the 10 meter Caltech Sub-millimeter Telescope (Enoch et al.

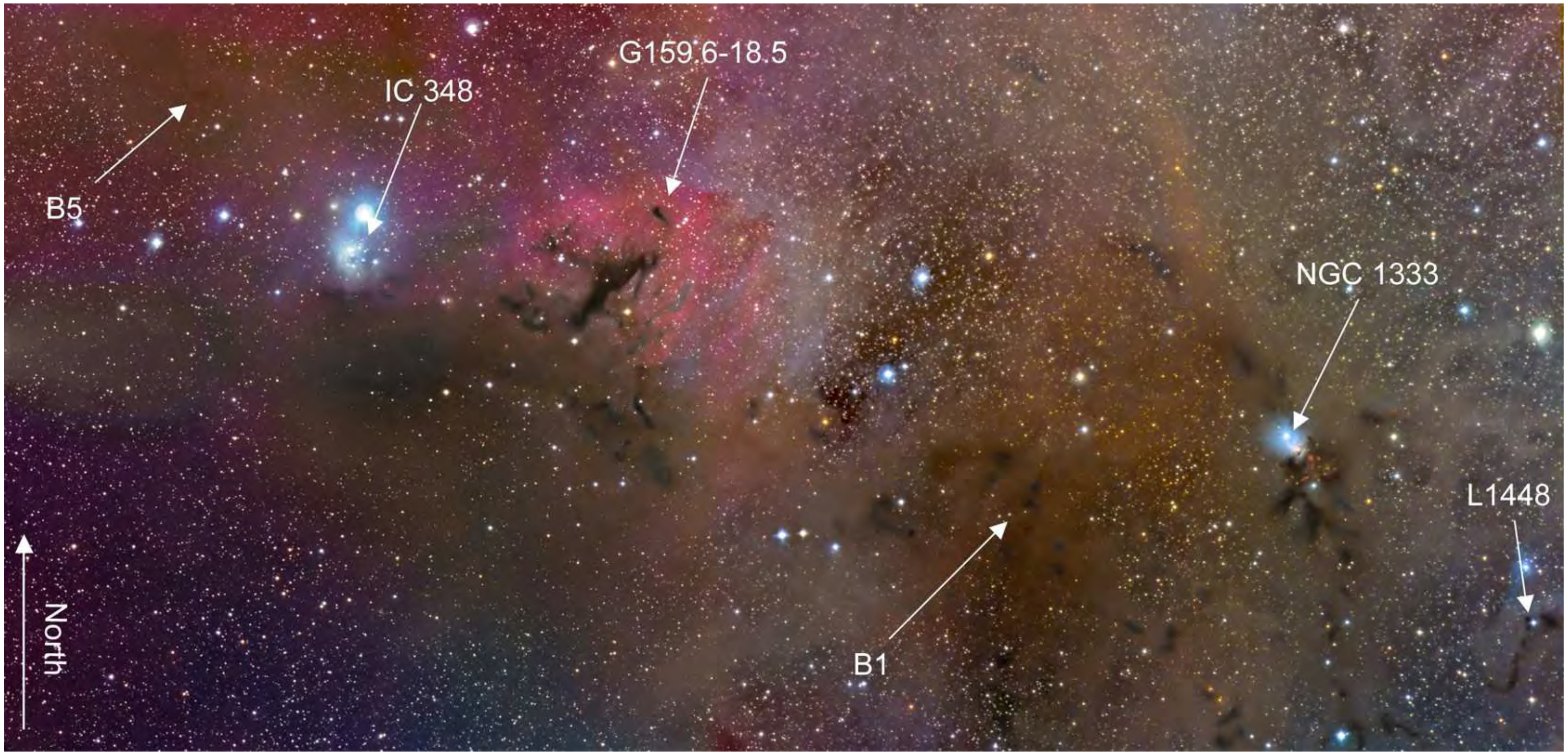

Figure 3. A visual wavelength image of the Perseus molecular cloud. This image was obtained by Adam Block.

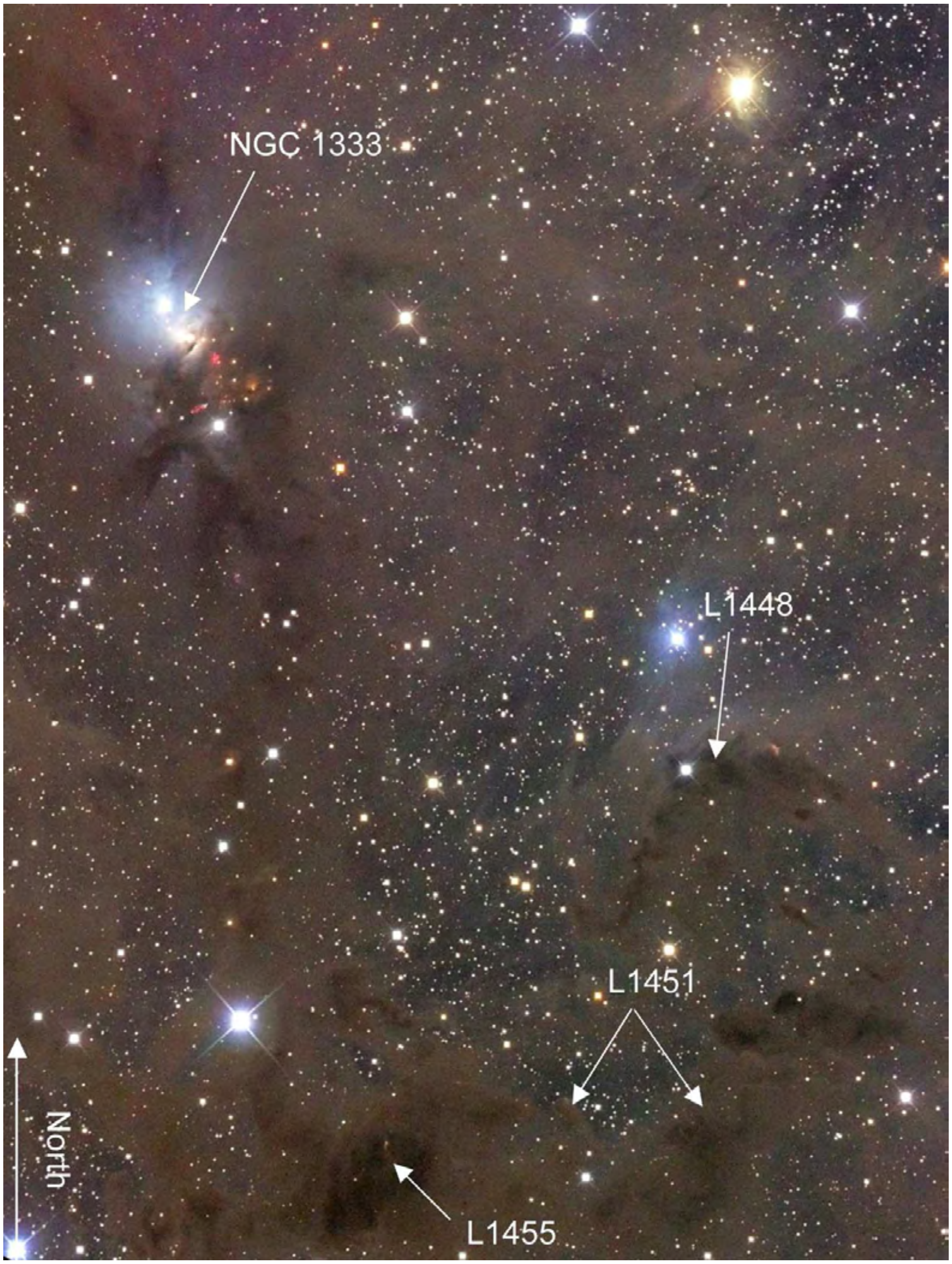

Figure 4. A visual wavelength image of the western portion of the Perseus molecular cloud. This image was obtained by Jeff Lunglhofer through broad-band RGB filters and an unfiltered luminance image.

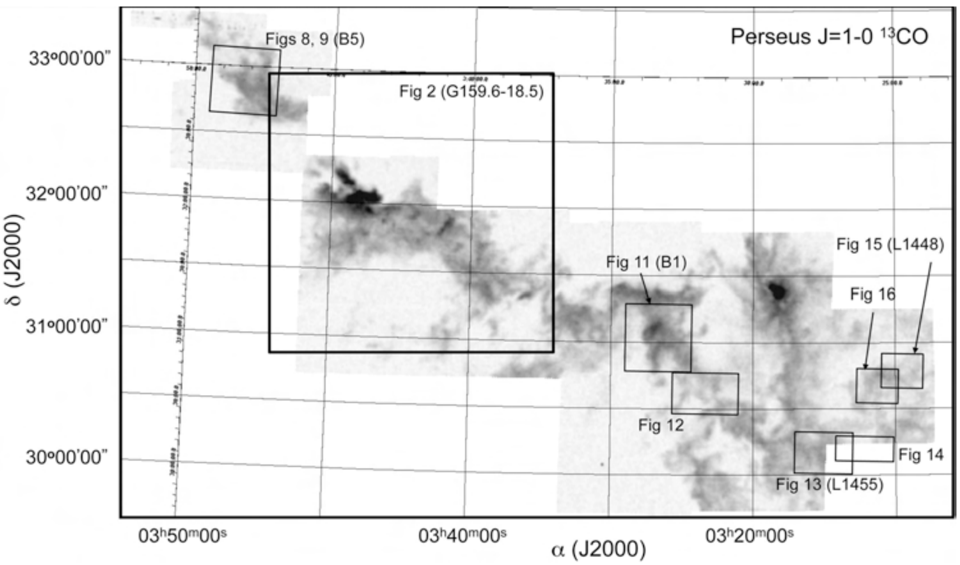

Figure 5. An image of the Perseus molecular cloud showing the peak antenna temperature of the 110 GHz J = 1 - 0 transition of ^{13}CO. The CO data, obtained with the Bell Laboratories 7 meter antenna in the mid-1980s, has an angular resolution of 100$''$. The boxes show the locations of various other figures in this chapter detailing outflows and other features in the Perseus cloud.

2006). Additionally, the entire cloud has been surveyed in narrow-band Hα and [SII] emission to search for outflows by means of their shock-excited Herbig-Haro emission (Walawender et al. 2005a and Figures 5 and 6). The entire Perseus cloud has also been surveyed with the infrared cameras on the Spitzer Space Telescope (Jørgensen et al. 2006). Individual regions such as Barnard 1, Barnard 5, NGC 1333, L1448, and L1455 have been the subject of extensive investigations at many wavelengths at a variety of resolutions, resulting in hundreds of citations.

There are several measurements of the distance to the Perseus molecular cloud. Herbig & Jones (1983) adopted a distance of 350 pc to the western end of the cloud (NGC 1333) based on several previous measurements primarily around the IC 348 cluster and the Per OB2 association. Černis, however, suggested a distance of 220 pc to NGC 1333 (Černis 1993) and 230 pc to Barnard 1 (Černis & Straižys 2003) based on interstellar extinction. Herbig (1998) adopted a distance of 316 pc to IC 348 on the east end of the Perseus cloud complex based on analysis of various measurements. However, it is possible that this cloud consists of several discrete components at different distances and that the various apparently discrepant distance determinations may thus be correct.

Hirota et al. (2008) used the VERA long-baseline array of radio telescopes to directly measure the distance to the SVS 13 source in the NGC 1333 cluster on the western end of the cloud by observing the parallax of a maser. The 22 GHz H_2O maser was found to have a distance of 235 $\pm$ 18 pc. This measurement provides the most reliable determination of the distance to the western portion of Perseus. Future radio parallax measurements may provide accurate measurements to other parts of the complex. Because various portions of the cloud may be at different distances, we adopt

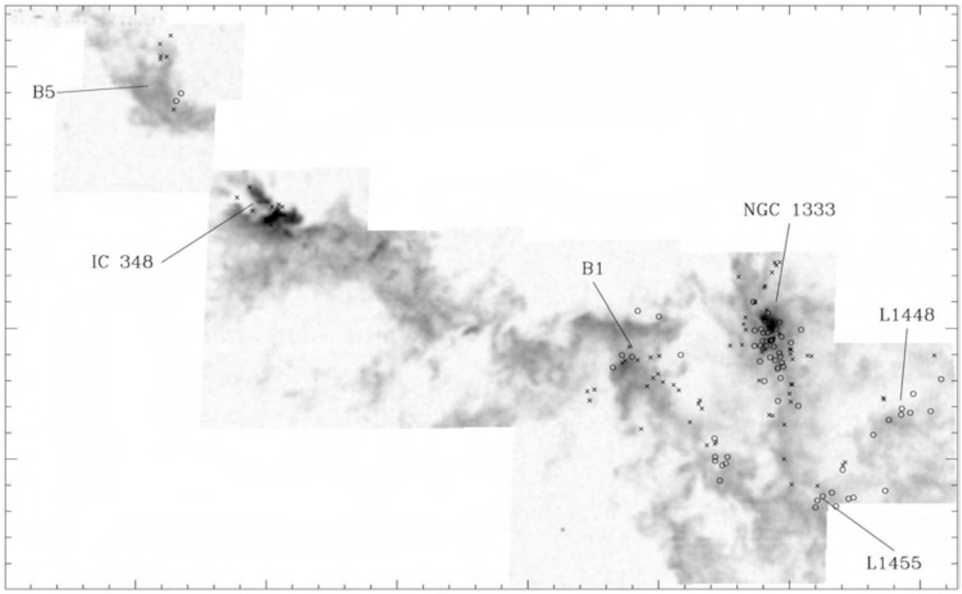

Figure 6. The Perseus molecular cloud showing the peak antenna temperature of the 110 GHz J = 1 - 0 transition of ^{13}CO. The circles show Herbig-Haro objects discovered prior to the Mosaic CCD survey of Hα and [SII] emission by Walawender et al. (2005a). The crosses show the new objects found in the Mosaic survey.

a value of 300 pc for the entire Perseus molecular cloud for calculations requiring a distance estimate.

The Perseus cloud has a mass of about $10^4 M_\odot$ (Ungerechts & Thaddeus 1987; Sancisi et al. 1974), an angular extent of about 1.5 by 5 degrees (8 by 25 pc), and is located west of the Per OB2 association. Bachiller & Cernicharo (1986b) determined a mass of 1.7×10^4 $M_\odot$ using a visual extinction map while Kirk et al. (2006) found a somewhat larger mass of 2.7×10^4 $M_\odot$ (when scaled to a distance of 300 pc) using near-infrared extinction map data.

The Perseus molecular cloud is a relatively low mass and small cloud compared with the typical giant molecular clouds in the Galaxy responsible for most on-going star formation. Observations show that it is currently only forming low- to intermediate-mass stars with spectral types later than about B1. CO maps show that the cloud structure is filamentary on scales ranging from arcminutes to degrees. Dense gas tracers and sub-mm continuum emission from dust indicate that cores mark the densest portions of these filaments (Hatchell et al. 2005; Enoch et al. 2006, Kirk et al. 2006). The eastern portion of Perseus contains the star forming cloud B5, a young cluster IC 348 (see the chapter by Herbst in this Handbook), and a large region devoid of obvious signs of active star formation also known as B4. As discussed above, a diffuse HII region and warm dust ring are located behind this region. The western portion of the cloud is marked by a large, 1.5° by 1° cavity rimmed by the dense star forming cores containing (in clockwise order) NGC 1333, L1455, IRAS 03272+3013, IRAS 03282+3035, and Barnard 1.

The Perseus molecular cloud exhibits a large velocity gradient. The eastern portion of the cloud at the location of Barnard 5 has V_{LSR} = 10.5 km s^{-1} while the western portion near L1448 has V_{LSR} = 2 km s^{-1}. There are three plausible explanations for this gradient: 1) the cloud may be rotating, 2) the cloud may consist of several components superimposed along the line-of-sight, or 3) it may be the result of differential acceleration by the Per OB2 association. If the velocity gradient were produced by gravitationally bound motion, the total mass of the cloud would have to be more than 4×10^4 M$_\odot$, at least a factor of 2 larger than the observed mass.

Inspection of the CO data cubes reveals several discrete velocity jumps in spatial velocity cuts. This structure could be easily explained if the cloud consists of several distinct, but lower mass clouds superimposed along the line-of-sight. This model could reconcile the larger than 300 pc distance found for the eastern portion of the cloud containing IC 348 (Herbig & Jones 1983) and the 220 pc distance to the western part containing NGC 1333 (Černis 1990, Hirota et al. 2008). The chance superposition of unrelated clouds along the line-of-sight is unlikely. The recent study by Ridge et al. (2005) provide some evidence for the multiple cloud scenario.

Like most molecular clouds, the Perseus cloud exhibits a complex and chaotic structure consisting of dense cloud cores surrounded by an interconnected network of filaments and sheets. Many voids surrounded by partial arcs or nearly complete rings are also seen. This complicated structure is one possible signature of supersonic turbulence. Indeed the line widths in CO are super-thermal. The line-width, velocity field, and cloud structure has been compared to numerical models of supersonic turbulent models of molecular clouds with excellent agreement (e.g., Padoan et al. 1999).

Investigation into the dense cores using dust continuum observations has revealed that the cores predominantly lie within high extinction regions of the larger cloud (Hatchell et al. 2005; Enoch et al. 2006; Kirk et al. 2006). Kirk et al. (2006) compare extinction observations of the cloud with the location of the cores and find an extinction threshold for core formation at $A_v = 5 - 7$. Interestingly, the cores do not appear randomly scattered about each region of high extinction. Rather they are often found offset from the peak of extinction. Considering the ensemble of cores, there is indirect evidence that 40 Per, or another member of the Per OB2 association, is influencing the next generation of stars in Perseus (Kirk et al. 2006). Assuming similar temperatures and dust properties for all the dust continuum cores, the mass function for the cores is similar to the stellar IMF (Enoch et al. 2006; Kirk et al. 2006). Combined with the observation that these cores account for $\sim$ 1% of the cloud mass and ~ 10% of the mass within each region of high extinction (Kirk et al. 2006) it appears that the core properties are very similar to the properties of young star clusters (Lada & Lada 2003).

Perseus was surveyed at 850 μm by Hatchell et al. (2005, 2007a, 2007b) and Hatchell & Fuller (2008) using SCUBA. They found 103 cores with masses ranging from 0.5 to 50 M$_\odot$. Hatchell et al. (2007a) used Spitzer mid-IR detections to determine whether their cores contained protostars and found that the ratio of protostellar cores to starless cores increases with mass. Hatchell et al. (2007b) looked for signatures of molecular outflows as a proxy for the presence of a protostar and found a similar result. Hatchell & Fuller (2008) found that in their sample of cores, the prestellar and protostellar cores have different mass distributions. They also find that their core mass function (CMF) is "inconsistent with an apparently simple, direct mapping of the CMF to IMF."

A study comparing the cores with and without embedded protostars was undertaken by Jørgensen et al. (2007) using both the Spitzer observations (Jørgensen et al.

2006) and the dust continuum observations (Kirk et al. 2006). Positive identification of 49 deeply embedded protostars was obtained, many being discovered through this multi-wavelength analysis. These protostars are located extremely close to the peak of the dust continuum measurement within each core, arguing against significant motions for these protostars.

Rosolowsky et al. (2008) present a multi-transition study of 193 dense cores and core candidates in Perseus using the 23 GHz lines of ammonia (NH_3) and the 22 GHz line of C_2S. The NH_3 emission closely traces the 1.1 mm dust continuum and exhibits line-widths ranging from 0.07 to 0.7 km s^{-1} with the most common value of about 0.15 km s^{-1}. These cores have a mean temperature of about 11 K.

Kirk, Johnstone, & Tafalla (2007) presented a survey of over 150 cores using the 93 GHz N_2H^+ as a tracer. Again, the majority of 0.85 mm and 1.1 mm continuum emitting cores are detected in this tracer (about 84%). A comparison between the dust and N_2H^+ column densities indicates that the abundance of this molecular ion is about 10^{-9} to 10^{-10} compared to H_2. The velocity differences between this ion and the surrounding molecular cloud as traced by $C^{18}O$ is less than the sound-speed in 90% of the cores, indicating that internal motions are mostly subsonic. However, the kinetic energy in these motions is sufficient to prevent gravitational collapse. As many previous studies have shown, starless cores tend to have smaller line-widths than those associated with YSOs. The N_2H^+ line-widths tend to increase with 0.85 mm flux and degree of central concentration of this flux. The presence of N_2H^+ also sets a minimum age of about 10^5 years for these cores. The one dimensional radial velocity dispersion of the core-to core motions within a given extinction region indicate that the N_2H^+ cores in each region tend to have sub-Virial motions. That is, the core-to-core variations in radial velocity appear to be considerably less than required to counter-balance the inward pull of gravity. Thus, the N_2H^+ cores in each extinction region may be experiencing orbit decay.

3.1. External Influences

The eastern portion of the cloud is located closer to the centroid of the Per OB2 association and may have been more severely impacted and accelerated by the combined effects of soft-UV, ionizing radiation, stellar winds, and supernova explosions. The overall velocity gradient implies that the kinetic energy imparted to the eastern part of the cloud must be at least 3×10^{48} ergs. This is not implausible given the HI supershell associated with the Perseus complex. This is the model advocated by Sun et al. (2006).

Although no massive stars earlier than B1 are currently forming from the remaining molecular gas in this region, about a dozen such stars were formed in the vicinity of the Perseus cloud in the Per OB2 association within the last 10 Myr (see Section 2.). The presence of the diffuse HII region G159.6-18.5 behind the cloud indicates that massive star formation occurred even more recently. Walawender et al. (2004) presented observations of the L1451 region which show that nearby massive members of Per OB2 have had a profound influence in shaping parts of the Perseus cloud. Walawender et al. (2004) found that the cloud core surrounding the young star IRAS 03235+3004 may have been shaped by UV radiation from the star 40 Per located about 25 pc away. The dust emission in the vicinity of Barnard 1 as well as some other SCUBA 850 μm cores throughout the Perseus complex show hints that dust clouds are triggered into star formation from the direction of this star (Kirk et al. 2006). Additionally, the several million year old IC 348 cluster located at the eastern end of the complex has been mostly cleared of dust and gas within a few parsecs of its most massive stars. Thus, UV radiation may have played a role in the generation of turbulent motions and cloud disruption in parts of the complex.

Today, most of the Perseus molecular cloud appears to be shielded from direct illumination of intense UV radiation fields, perhaps because the most massive members of Per OB2 have evolved off the main sequence. Over most of the projected surface area of the cloud, there are no obvious ionization fronts or other signs of significant UV illumination that could energize or destroy the cloud complex. However the Spitzer MIPS scan-maps of 24 and 70 μm emission do show that the IC 348 region and the portions of the molecular cloud immediately south of G159.6-18.5 contain warm dust most likely heated by soft-UV radiation fields of the early B stars in the region.

3.2. The Magnetic Field

The magnetic field structure of the Perseus molecular cloud has been investigated by both the linear polarization of background starlight (Goodman et al. 1990) and by means of Zeeman splitting (Goodman et al. 1989). Barnard 1 is also the first dark cloud for which OH Zeeman measurements yielded a positive result (see Section 4.5).

The results of visual-wavelength polarization measurements over the entire extent of the Perseus cloud are shown superimposed on the IRAS-derived dust column density in Figure 3.2.. The IRAS-derived dust map traces primarily the warm dust surrounding young stars in regions such as NGC 1333, IC 348, and the low-surface brightness HII region G159.6-18.5. This figure shows that the stars exhibiting large polarization (P $>$ 1.2%) predominantly exhibit polarization orientations from southeast to northwest. The lower amplitude polarization vectors are aligned nearly orthogonal to this orientation. Arce et al. (1998) have argued that the polarization efficiency of dust associated with cold molecular gas is considerably lower than the efficiency of dust embedded in warm atomic gas. Thus, it is tempting to argue that the high-polarization in Perseus is predominantly associated with the warm dust surrounding the HII region G159.6-18.5 that is well traced by the IRAS-derived dust column density shown in Figure 3.2.. The low-polarization vectors may mostly trace magnetic fields associated with the Perseus cloud itself. Thus, in the dust surrounding the HII region, the magnetic field may be mostly parallel to the ionization front. On the other hand, the mean magnetic field direction in the molecular cloud appears to be aligned with the major axis of the cloud.

3.3. Overview of the YSOs in Perseus

The Perseus molecular cloud contains hundreds of YSOs identified by the Spitzer Space Telescope. However, in discussing Spitzer YSOs, it is important to remember that Spitzer observations tend to select YSOs in either their Class I or II stages of evolution. The younger Class 0 sources tend not to be visible in the IRAC images while the older Class III and weak-line T Tauri stars tend to be hard to distinguish from the hundreds of thousands of main sequence stars along the line of sight. Thus, both the currently forming stars, and the older population of pre-main sequence objects are under-represented in the Spitzer surveys.

The less than 5 Myr old cluster IC 348 contains over 420 young stars, most of which are Class II or III YSOs (Muench et al. 2007; see chapter by Herbst). The much younger and still forming NGC 1333 cluster contains at least 150 YSOs, many of which as still embedded Class 0, I, or flat spectrum sources (see chapter by Walawender et al.). In addition to these large clusters, smaller aggregates of stars are associated with the

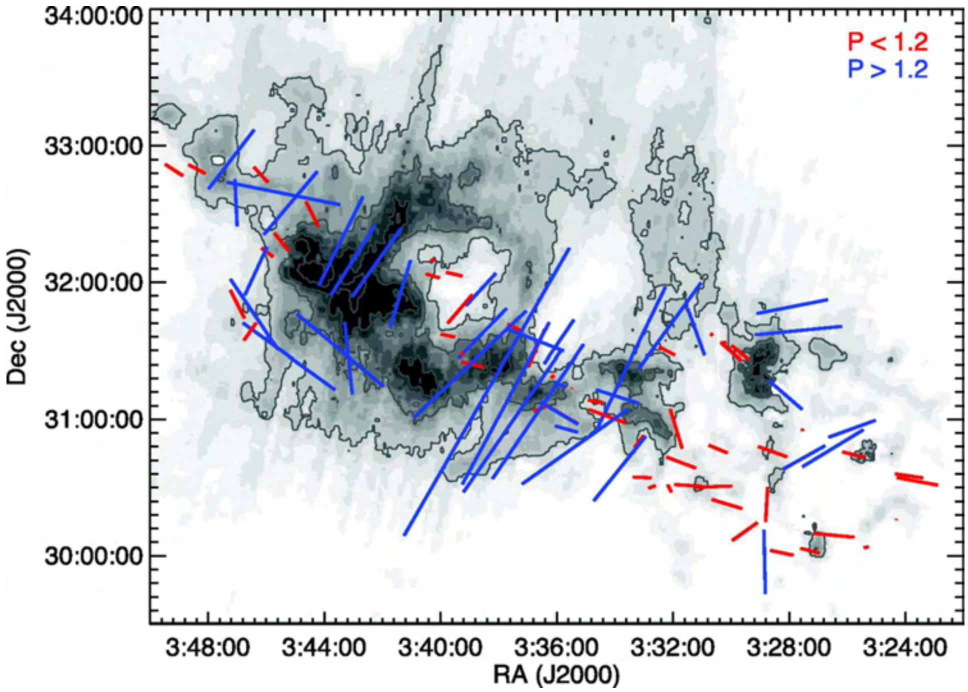

Figure 7. IRAS-derived dust column density overlaid with polarization vectors from Goodman et al. (1990). The polarization vectors shown are parallel to the orientation of the magnetic field in the plane of the sky. Blue vectors have polarization strength P $>$ 1.2% and red vectors have P $<$ 1.2%. The stronger polarization may trace warm dust associated with the IRAS dust (courtesy of the COMPLETE team).

major cores such as B1, L1448, and L1455, and some additional YSOs are located in the remaining portions of the cloud.

Jørgensen et al. (2006) identified about 400 YSOs in the Perseus molecular cloud using Spitzer / IRAC observations. However, the more recent, and wider-field census of IC 348 by Muench et al. (2007) found a larger number of YSOs (about 420) in IC 348 alone. Thus, the Jørgensen et al. 400 sources are a lower bound to the actual number of Spitzer-selected YSOs. About two-thirds of these sources are associated with the major clusters IC 348 and NGC 1333. The remaining one-third of the YSOs constitute a distributed population in the Perseus cloud. But of these, over half (one-sixth of the total) are parts of the smaller aggregates found in B1, L1448, and L1455. About two-thirds of the YSOs are classified as Class II objects with the remaining one-third being either Class I or ”flat-spectrum” objects. The percentage of Class I and ”flat spectrum” objects varies from 14%, to 26%, to 47% in IC 348, NGC 1333, and in the distributed portions of the cloud, respectively. These percentages are consistent with the suspected ages of the two major clusters with IC 348 being older than NGC 1333.

A survey of the embedded YSOs in Perseus was undertaken by Jørgensen et al. (2007). By combining extremely red IRAC protostars and MIPS sources coincident with sub-mm SCUBA cores (coincident within 15″) a list of 49 embedded objects was tabulated for the entire Perseus molecular cloud (Table 1). Most of these protostars were found very close to the peak of the sub-mm cores, implying that the majority of these sources have not moved significantly relative to their cloud cores during their formation. Thus these cores are not very dynamic.

It is interesting that the Class I and ”flat spectrum” sources are relatively more common amongst the distributed population of YSOs in the Perseus cloud than in the two major clusters. One possible explanation for this dichotomy is that in the clusters, YSOs tend to lose their envelopes more rapidly. Three mechanisms may contribute to the relatively fast removal of envelopes in clusters. First, the soft-UV radiation emitted by the late B and A type members can heat cloud surfaces and lead to soft-UV dominated photo-evaporation. Second, the cumulative impact of multiple outflows may mechanically strip the outer portions of cloud cores. Third, dynamical stripping by close encounters with sibling stars are more likely to strip envelopes in a cluster than in the field. These mechanisms do not operate for isolated stars and tend to be much less effective for small aggregates. Thus, cluster YSOs may emerge from their birth cocoons more rapidly than stars born in isolation.

3.4. Overview and Impact of Outflow Activity

Protostellar winds and jets are one of the easiest manifestations to observe of the birth of a young star. Before the launch of the Infrared Space Observatory (ISO) and the Spitzer Space Telescope, the most embedded and youngest protostars were often found first by means of their bipolar outflows. The discovery of the Class 0 source L1448 C (see below), which was not listed in the IRAS point source catalog, provides a good example. This CO outflow was discovered by Bachiller et al. (1990a) during their investigation of high velocity gas around the nearby infrared source IRS 3 in the L1448 region. However, high resolution mapping of CO with the IRAM 30 meter telescope revealed that the dominant high velocity outflow in the region has kinematic symmetry about another location where no IR source had yet been found. Dubbed the ”U-star” by Bachiller et al. (1990a), this source was subsequently detected at mm and sub-mm wavelengths to become one of the first ”Class-0” protostars. Subsequent studies demonstrated that all three IRAS sources drive their own outflows and that IRS 3 is a multiple star system with each member driving its own outflow.

Hatchell, et al. (2007b) presented the first comprehensive survey of molecular outflows from dense cloud cores that covers the entire Perseus cloud. They found broad CO J = 3–2 line-wings indicative of molecular outflows from 37 of 51 cores they investigated. The first complete survey of visual wavelength shocks (Herbig-Haro objects) in the Perseus cloud was presented by Walawender et al. (2005b). These narrow-band images revealed the presence of hundreds of individual shocks throughout the Perseus cloud. Many studies of individual outflows or groups of flows from various portions of Perseus have been conducted and will be presented in the discussion of individual regions below.

The origins of random, turbulent motions, and their relation to cloud structure has been extensively investigated in the Perseus cloud. There are two schools of thought about the origin of such motions: First, such motions might be inherited from a turbulent cascade originating from large (10 to $>$100 pc) scales. Second, feedback from young stars may inject energy and momentum into the cloud on small (1 to 10 pc) scales. In the first model, large-scale motion may be produced by supernovae, superbubbles, the acceleration by the gravitational potential of a passing spiral arm of the

Table 1. List of Embedded YSOs in Perseus from Jørgensen et al. (2007)[a]

No.	α_{2000}	δ_{2000}	Associated sources
1	$03^h25^m22.36^s$	$+30°45'13.6''$	L1448-IRS 2 / IRAS 03222+3034
2	$03^h25^m36.48^s$	$+30°45'23.2''$	L1448-N(A)
3	$03^h25^m38.87^s$	$+30°44'06.0''$	L1448-C(N)
4	$03^h26^m37.46^s$	$+30°15'28.2''$	
5.	$03^h27^m38.27^s$	$+30°13'58.5''$	L1455-FIR2
6	$03^h27^m39.11^s$	$+30°13'02.8''$	L1455-IRS 1 / IRAS 03245+3002
7	$03^h27^m43.25^s$	$+30°12'28.9''$	L1455-IRS 4
8	$03^h27^m47.69^s$	$+30°12'04.4''$	RNO 15 / FIR-03245+3002
9	$03^h28^m32.55^s$	$+31°11'04.8''$	
10	$03^h28^m34.53^s$	$+31°07'05.5''$	
11	$03^h28^m37.11^s$	$+31°13'28.3''$	IRAS 03255+3103
12	$03^h28^m39.11^s$	$+31°06'01.6''$	(ass. HH 340)
13	$03^h28^m40.62^s$	$+31°17'56.5''$	
14	$03^h28^m45.31^s$	$+31°05'41.9''$	IRAS 03256+3055
15	$03^h28^m55.59^s$	$+31°14'37.5''$	NGC 1333 IRAS-2A
16	$03^h28^m57.36^s$	$+31°14'15.9''$	NGC 1333 IRSA-2B
17	$03^h28^m59.55^s$	$+31°21'46.7''$	
18	$03^h29^m00.61^s$	$+31°12'00.4''$	
19	$03^h29^m01.66^s$	$+31°20'28.5''$	(ass. SVS 12/ASR 114)
20	$03^h29^m03.30^s$	$+31°15'55.5''$	NGC 1333 SVS-13
21	$03^h29^m04.09^s$	$+31°14'46.6''$	HH 7-11 MMS6
22	$03^h29^m10.53^s$	$+31°13'30.7''$	NGC 1333 IRAS-4A
23	$03^h29^m10.72^s$	$+31°18'20.5''$	
24	$03^h29^m11.29^s$	$+31°18'31.3''$	
25	$03^h29^m12.07^s$	$+31°13'01.8''$	NGC 1333-IRAS 4Bf
26	$03^h29^m13.62^s$	$+31°13'57.9''$	NGC 1333-IRAS 4C
27	$03^h29^m17.21^s$	$+31°27'46.2''$	(ass. Per 4)
28	$03^h29^m18.25^s$	$+31°23'19.9''$	(ass. HH 335)
29	$03^h29^m18.73^s$	$+31°23'25.4''$	
30	$03^h29^m23.50^s$	$+31°33'29.4''$	IRAS 03262+3123
31	$03^h29^m51.89^s$	$+31°39'05.6''$	IRAS 03267+3128/(Per 5) 2
32	$03^h31^m21.01^s$	$+30°45'30.0''$	IRAS 03282+3035
33	$03^h32^m18.03^s$	$+30°49'46.9''$	IRAS 03292+3039
34	$03^h33^m13.81^s$	$+31°20'05.2''$	(ass.Per 9B)
35	$03^h33^m14.41^s$	$+31°07'10.8''$	B1-SMM3
36	$03^h33^m16.49^s$	$+31°06'52.3''$	B1-d
37	$03^h33^m16.67^s$	$+31°07'55.1''$	B1-a / IRAS 03301+3057 / SMM6
38	$03^h33^m17.87^s$	$+31°09'31.8''$	B1-c / SMM2
39	$03^h33^m20.34^s$	$+31°07'21.4''$	B1-b / SMM1
40	$03^h33^m27.31^s$	$+31°07'10.2''$	(ass. HH 789) SMM 11
41	$03^h43^m50.99^s$	$+32°03'24.7''$	
42	$03^h43^m51.03^s$	$+32°03'08.0''$	
43	$03^h43^m56.91^s$	$+32°03'04.2''$	IC 348-MMS
44	$03^h43^m57.32^s$	$+32°00'47.6''$	HH 211-FIR
45	$03^h43^m57.64^s$	$+32°00'44.8''$	(ass. HH 211?)
46	$03^h43^m59.41^s$	$+32°00'35.5''$	(ass. HH 211?)
47	$03^h44^m02.40^s$	$+32°02'04.7''$	
48	$03^h44^m43.32^s$	$+32°01'31.6''$	IRAS 03415+3152
49	$03^h47^m41.61^s$	$+32°51'43.9''$	IRS 1/ IRAS 03445+3242

[a] Spitzer fluxes and other details can be found in Jørgensen et al. (2007).

Galaxy, or the infall of gas from above or below the Galactic plane. This forcing can accelerate, sweep-up, and compress low density, mostly atomic interstellar gas. Compression by convergent flows aided by gravitational instability can lead to the formation of turbulent, gravitationally bound molecular clouds. In this scenario, the observed highly supersonic motions within clouds, and the Larson scaling relationships between spectral line width and line central velocity with separation, are the result of a turbulent cascade of energy and vorticity from large to small scales (Padoan & Nordlund 1999; Miesch et al. 1999; Padoan et al. 2001; 2003). Miesch & Bally (1994) noted that the UV radiation and stellar winds of massive stars may also accelerate cloud surfaces and generate supersonic cloud motions.

The discovery of parsec-scale outflows from young stars, and the large amount of outflow activity in cluster-forming cloud cores such as NGC 1333 suggests that jets and winds from forming stars may make a major contribution to the energy and momentum budget of star-forming clouds. However, Basu & Murali (2001) have argued that protostellar outflows can not drive the large scale-turbulent motions within molecular clouds. The rate at which turbulent energy is dissipated depends inversely on the driving-scale of the turbulence. Using an outflow driving scale of 0.1 to about 1 pc, Basu & Murali argue that this driving scale implies a total (bolometric) luminosity of molecular clouds about 10^3 to 10^4 times their J = 1 – 0 ^{12}CO luminosity. Detailed models of molecular line cooling imply that this ratio is in the range 10 to 100. Furthermore, they claim that to drive the observed turbulence, the Galactic star formation rate would have to be one to two orders of magnitude greater than observed. Thus, protostellar outflows may not dominate the generation of turbulent motions on the scale of entire giant molecular clouds.

Nevertheless, in the absence of massive stars, outflows appear to play a dominant role in determining the structure and kinematics of random motions in star-forming cloud cores on a scale of 0.1 to a few parsecs. Outflows can disrupt such cores and therefore make an important contribution to the self-regulation of star formation by blowing away material that would otherwise be accreted by the stars. The random orientations of outflows results in random cloud structure and motions that resemble turbulence. However, when a region produces massive stars, the combined effects of their UV radiation, stellar winds, and supernova explosions completely overwhelms the impact of protostellar outflows. There has been no massive star formation in Perseus within the last few million years, making it an ideal laboratory for investigating the impacts of outflows.

The large number of shocks in the NGC 1333 region led Bally, Devine, & Reipurth (1996) to suggest that a typical random location in the parent cloud may be impacted by hard shocks every 10^4 to 10^5 years. Such shocks will heat, dissociate, and accelerate gas in the star forming region and effectively reset the chemical evolution of the impacted region to a primitive chemical state. Most of the outflow energy is radiated away. Slow shocks with speeds less than about 20 km s^{-1} radiate most of their energy in the near- to mid-infrared lines of species such as H_2 and fine-structure cooling lines. Faster shocks produce shorter wavelength (visual, UV, and soft X-ray) radiation that tends to be absorbed by dust and re-radiated in the far-IR/sub-mm continuum. The luminosity radiated away in the near- and mid-IR or by dust continua was not considered by Basu and Murali (2001) in their evaluation of the role of outflows in turbulence generation.

The NGC 1333 region is currently the most active site of on-going star formation in Perseus. The outflow activity in this region provides one of the clearest examples of the possible self-regulation of star formation by outflows. Bally et al. (1996) suggested that the NGC 1333 region represented a ‘micro-burst’ of star formation where the surface density of optically visible shocks is very high, ranging from an area covering factor of a few to many tens of percent. Bally et al. estimated that these shocks trace a sufficiently high energy deposition rate into the surviving molecular cloud to totally disrupt the remaining gas on a time scale less than 10^5 years. However, this estimate failed to correct for those flows which have burst completely out of the cloud and are therefore not depositing energy or momentum into it.

Sandell & Knee (2001) also found that outflows play an important role in the energy balance of NGC 1333. NGC 1333 has a filamentary cloud structure, consisting of many cavities, some of which can be traced to the action of current outflows and some which may be the remnants of past outflow activity. Sandell & Knee (2001) proposed that star formation may occur in density enhancements at the periphery of these cavities. Thus star formation may be triggered by previous episodes of star formation and associated outflow activity.

The survival time of a cloud in the presence of virulent outflow activity can be estimated by dividing the ”momentum content” of the cloud by the outflow momentum injection rate. Although there is growing evidence that low levels of outflow activity can persist for millions of years after the birth of a star, most of their momentum injection occurs early-on during the most active phase of protostellar accretion. Thus, the ”effective outflow lifetime” during which they inject most of their momentum must be around 10^5 years, the approximate average duration of the Class 0 and I phases of YSO evolution. Assume that a typical outflow has momentum $P \sim 10\,\mathrm{M}_\odot\,\mathrm{km\,s}^{-1}$, mechanical luminosity $L \sim 0.1\ L_\odot$, that it lasts about 10^5 years, and that on average there are about 10 such outflows operating at any one time in a region such as NGC 1333. The implied momentum injection rate is thus $\dot{P} \sim 10^{-3}\ \mathrm{M}_\odot\ \mathrm{km\ s}^{-1}\ \mathrm{yr}^{-1}$.

If the cloud has a mass of 150 $\mathrm{M}_\odot$ and a velocity dispersion of 2 $\mathrm{km\ s}^{-1}$, the momentum content of the cloud is 300 $\mathrm{M}_\odot\ \mathrm{km\ s}^{-1}$. The lifetime of the cloud is then given by $\tau = P/f\dot{P} = 3 \times 10^5/f$ years. where f is the efficiency with which the outflow momentum is coupled back into the cloud. If all outflows are trapped, then $f = 1$ and the cluster core can be disrupted in about $\tau = 3{\times}10^5$ years. But observations show that many outflows burst out of their birth environments. If $f = 0.1$, then the cloud disruption time-scale increases to about 3 Myr for these parameters.

Walawender et al. (2005a) used a global survey of Hα and [SII] emission to identify Herbig-Haro objects which trace currently active shocks in outflows. They compared the energy and momentum traced by these shocks with the total turbulent kinetic energy and momentum in the Perseus clouds as traced by CO observations. Walawender et al. (2005a) also analyzed the amount of energy and momentum injected by molecular outflows. The results of these preliminary analyses can be summarized as follows: Outflows can inject more than sufficient energy and momentum to drive turbulence motions and even to disrupt individual cloud cores such as NGC 1333. Thus, outflows can self-regulate star formation and even disrupt surviving portions of the cloud core in regions such as NGC 1333. However, on the scale of the entire 10^4 $\mathrm{M}_\odot$ GMC, outflows may fail by nearly an order of magnitude to re-supply the momentum being dissipated by the decay of turbulent energy. Thus, while being able to self-regulate star formation on the scale of individual cloud cores containing a few hundred solar masses, outflows can not supply the random motions observed on large scales. To maintain a steady state, other sources of energy are required. These include acceleration of the cloud by soft-UV photo-heating, or ionization by hard-UV, the impact of massive star winds and supernova explosions, or the injection of turbulent energy from large-scale flows such as the supershell, or the impact of other clouds.

4. Individual Regions in the Perseus Cloud

We now discuss the most prominent individual star forming regions within the Perseus cloud. From east to west, these include Barnard 5, IC 348 (discussed in the chapter by Herbst), the HH 211 region adjacent to IC 348, Barnard 1, NGC 1333 (discussed in the chapter by Walawender et al.), L1455, and L1448.

4.1. Barnard 5

Barnard 5 (B5 for short; Figures 3, 5, 8, and 9), located at the far eastern end of the Perseus molecular cloud is one of the most extensively studied dark clouds in the sky

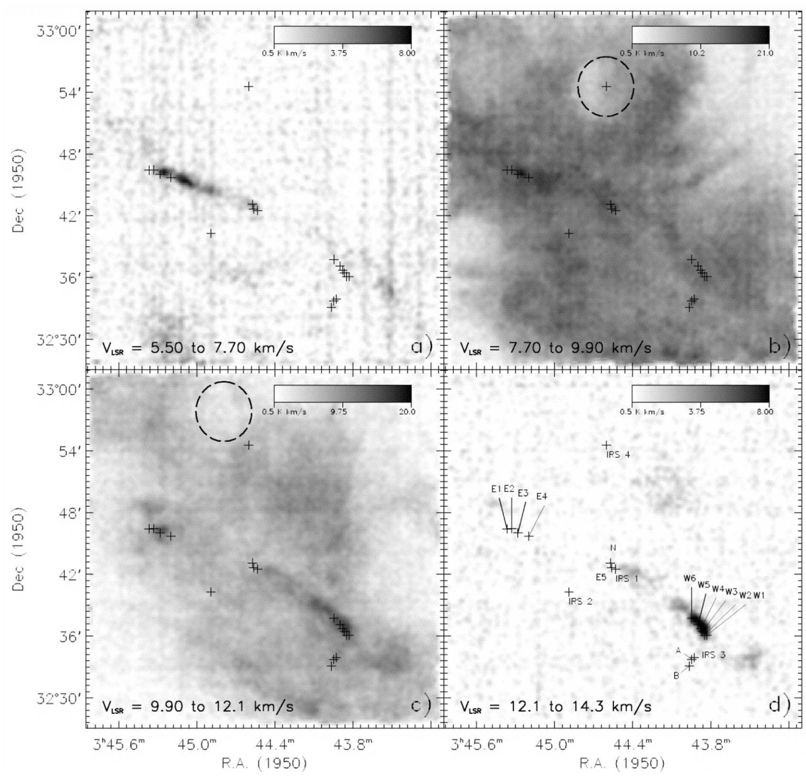

Figure 8. J = 2-1 230 GHz images of Barnard 5 and the HH 366 outflow taken from Yu, Billawala, & Bally (1999). The upper-left panel shows the blueshifted lobe of the HH 366 outflow from B5 IRS1. The upper-right panel shows low-velocity blue-shifted velociteis close to the cloud core and the lower-left panel shows the low velocity red-shifted emission. The lower-right panel shows the redshifted CO emsision. Various visual-wavelength knots in Figure 10 are labeled in this panel. The dashed circle in the upper-right and lower-left panels show the outline of a prominent cavity in the visual wavelength images through which background galaxies can be easily seen.

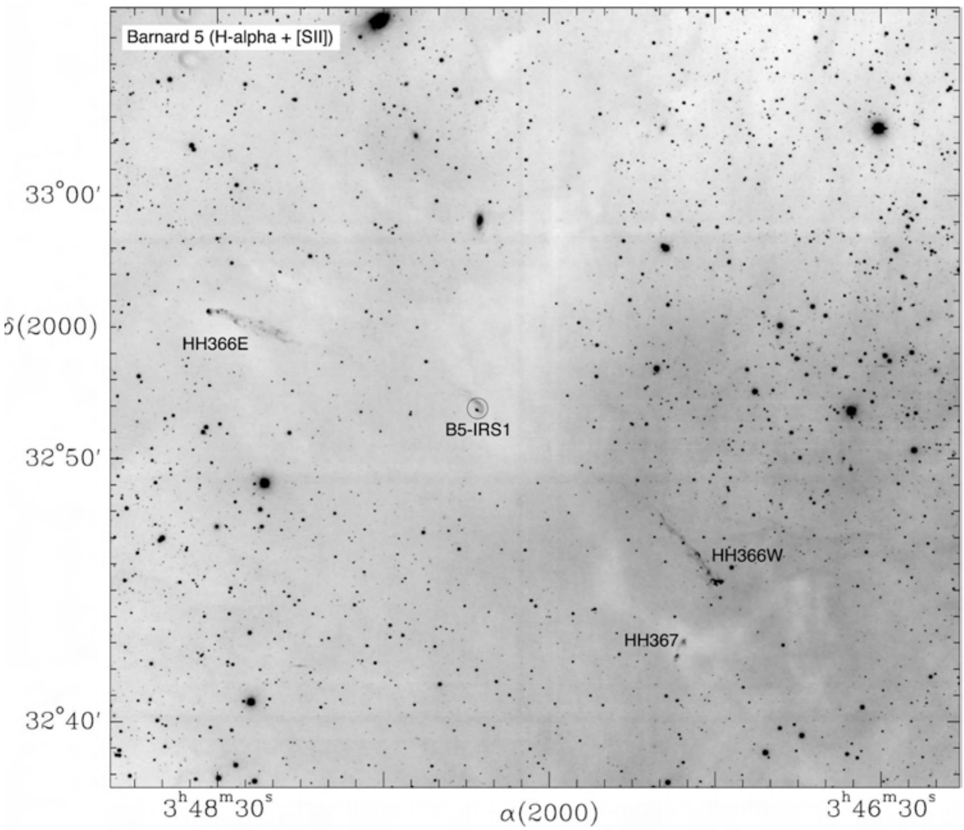

Figure 9. An Hα plus [SII] image of HH 366 in the B5 cloud (Bally, Devine, & Alten 1996) as observed in 2001 with the Mosaic CCD on the Mayall 4 meter reflector on Kitt Peak. Note the C-shaped bend of this outflow.

with well over 100 references. B5 has a total mass of approximately 10^3 $M_\odot$ (Stenholm 1985; Goldsmith, Langer, & Wilson 1986; Langer et al. 1989). The cloud contains several dense cores (Fuller et al. 1991; Olmi, Testi, & Sargent 2005; Hatchell et al. 2005; Kirk et al. 2006), exhibits limb-brightening in CO indicative of a cold cloud interior surrounded by a photo-heated exterior (Beichman et al. 1988), and evidence for large dust grains (Bhatt 1986).

Although a fairly massive dark cloud, B5 contains only a few IRAS sources, YSOs, and outflows. The brightest IRAS source, IRS1, is one of the first embedded YSOs to be carefully analyzed using the IRAS data (Beichman et al. 1984). IRS1 is surrounded by a dense circumstellar disk, a biconical reflection nebula, and an axial jet. Both infall through the disk, and outflow in bipolar cavities are observed simultaneously (Langer, Velusamy, & Xie 1996). The IRS1 protostar drives a parsec-scale outflow (Goldsmith et al. 1986; Bally, Devine, & Alten 1996). The low-velocity CO emission is concentrated along the walls of bipolar outflow cavities which extend over the length of B5 (about 20′) but are less than 1′ wide (Figure 8). This highly collimated outflow exhibits a pronounced C-shaped bend which can be explained by a 5 to 10 km s^{-1} motion of IRS1 towards the northwest with respect to the bulk of gas in B5. Alternatively, the gas may be flowing past IRS1 towards the southeast, consistent with the triggering vector found by Kirk et al. (2006). Several low-velocity CO bow-shocks are seen towards the ends of the CO outflow which have been interpreted as the swept-up partial shells associated with earlier eruptions of IRS1. Herbig-Haro objects and shock-excited H_2 emission are seen interior to the limb-brightened walls of the CO outflow along the entire length of the IRS1 outflow. These HH objects are collectively designated HH 366E and HH 366W (Yu, Billawala, & Bally 1999; Figure 9).

A second, smaller flow is driven by IRS3, located southwest of IRS1 towards the southwestern lobe of the IRS1 flow. A small Herbig-Haro object in this flow, HH 367, traces an internal working surface. The HH survey of Walawender, Bally, & Reipurth (2005a) found an additional Herbig-Haro object, HH 844, along this flow axis. Several HH objects north of the parsec scale HH 366 flow indicate additional outflow activity from as yet unidentified sources. Indeed, the molecular line maps of B5 show that there is a large hole in the cloud along its northern rim through which distant galaxies can be seen. This may trace an ancient outflow cavity.

4.2. IC 348

At the east end of the Perseus cloud (Figures 3 and 5), the IC 348 cluster contains several hundred members. The IC 348 cluster and its population of young stars is reviewed by Herbst in this Handbook. Here we summarize the relationship of this cluster to the Perseus molecular cloud and the Per OB2 association. Herbig (1998) found that the Hα emission line stars in IC 348 have a spread of ages from about 0.7 to 12 Myr. Luhman et al. (1998) concluded that most of the star formation in IC 348 took place within the last 3 Myr, but that some stars in this region formed 10 Myr ago. However, Muench et al. (2003) found that IC 348 had a mean age of $\sim$2 Myr with a spread of $\sim$3 Myr, corresponding to an epoch of roughly constant star formation rate between 0.5 and 3.5 Myr ago. In addition, Luhman et al. (1998) find that stars in IC 348 have a lower disk fraction than many other young clusters, indicating that stars in IC 348 are old enough to have mostly lost their disks. There are only a few active protostellar outflows in the IC 348 region. Thus, IC 348 appears to be an example of a region which is at or near the end of its star forming phase. The apparent age spread in IC 348 may be an indication that two episodes of star formation have occurred in the IC 348 region. While the younger stars must represent an intense burst of star formation that occurred within the last few million years from a now dissolved core in the Perseus cloud, the older generation may trace low-mass members of the Per OB2 association rather than a previous generation of star formation in IC 348.

It may be significant that the IC 348 region is located at the eastern end of the Perseus cloud which is closest to the centroid of the HI supershell and OB association. IC 348 may have been the first part of the Perseus cloud to experience triggered star formation. Regions located to the west are expected to be younger, as supported by observations.

4.3. Star Formation Southwest of IC 348

The dense cloud core located $10'$ southwest of IC 348 is one of the brightest in integrated ^{13}CO emission in the entire Perseus molecular cloud complex (e.g. Walawender et. al. 2005a). This cloud core is associated with an optical and near-IR reflection nebula which Boulard et al. (1995) named the “Flying Ghost Nebula”. Strom, Strom, & Carrasco (1974) found a near-IR source (IC 348 IR) with colors consistent with a deeply embedded B star which is probably illuminating the nebula. Based on the comparison between models and the appearance of a disk shadow in the reflection nebula, Boulard et al. (1995) concluded that the appearance of the "Flying Ghost Nebula" and photometry of its central star could be produced by a B7.5 star behind 28-36 magnitudes of visual extinction with a disk of radius 2400 AU (scaled to the 300 pc distance used here) and mass of 0.03 $M_{\odot}$. However, Avila, Rodríguez, & Curiel (2001) used the VLA at 3.5 cm and 7 mm to study this same source and concluded that the disk must be much smaller ($r_{\rm disk} < 10$ AU) with a mass of 0.05 $M_{\odot}$.

Approximately 1′ south of IC 348 IR, McCaughrean, Rayner, and Zinnecker (1988) discovered a highly collimated outflow (HH 211) by means of its shock excited molecular hydrogen emission. Eislöffel et al. (2003), using 1.2 mm continuum emission, discovered HH 211-mm, the driving source for the HH 211 outflow. HH 211-mm is not visible at near-IR wavelengths, thus it is likely a Class-0 protostar. This highly collimated jet-like flow was imaged in SiO with the VLA by Chandler & Richer (2001) and in CO by Gueth & Guilloteau (1999). Walawender et al. (2005a) found visual wavelength emission from HH 211, making it a bona-fide Herbig-Haro object as defined by optical emission.

McCaughrean, Rayner, and Zinnecker (1988) also found a chain of H_2 knots north of HH 211. Eislöffel et al. (2003) found the southern extension of this north-south flow and identified a candidate driving source (IC 348 MMS) which is bright in the submillimeter, but not visible in the near-IR, indicating that it is also a Class-0 source.

Walawender et al. (2005a, 2006) found a dozen new HH objects near HH 211 and south of IC 348. Thus, there is a small embedded cluster of forming stars near HH 211 in the region south of IC 348. This region is comparable in outflow activity to other sites of distributed star formation in Perseus such as L1448 and L1455. It is possible that star formation in this region was triggered by action of the now mostly inactive young stars in the IC 348 cluster. Winds and outflows from IC 348 may have compressed the surrounding material and triggered core collapse. Star formation in the HH 211 region may also have been influenced by the expansion of the IRAS dust ring associated with G159.6-18.5 and HD 278942. It is possible that molecular gas in this region was compressed from two directions, leading to gravitational collapse.

4.4. The Zone Between IC 348 and Barnard 1

The 1.5° portion of the Perseus molecular cloud between IC 348, and the dense core Barnard 1, 1.5° to the west, appears to be relatively devoid of on-going or very recent star formation, but does contain quite a few Class II YSOs and possible evidence for molecular outflows. However, the survey of Walawender et al. (2005a) found no Herbig-Haro objects in this portion of the cloud, indicating that there are no bright shocks on the near surface of the cloud. However, the Spitzer IRAC survey of Jørgensen et al. (2006) did find several dozen candidate Class II YSOs and even several Class I objects here. The Class II stars may trace outlying portions of the IC 348 cluster, or possibly signify an earlier episode of low-mass star formation that was followed by a period of relative inactivity.

The cloud structure, radial velocity field, and line-width are similar to other, more actively star-forming parts of Perseus. The cloud is filamentary, clumpy, and exhibits chaotic turbulent motions. The extinction in this region remains high with area-averaged A_V up to 6 - 8 magnitudes. The main distinction between this portion of Perseus and those which are actively forming stars is the absence of massive dense cores. There are no bright SCUBA sub-mm or Bolocam 1.1 mm cores (Hatchell et al. 2005; Kirk et al.

2006; Enoch et al. 2006) in this part of the cloud. There are, however, some very faint 1.1 mm cores with fluxes below about 100 mJy and masses smaller than 1 $M_{\odot}$. These small cores may be either pre-stellar or in the very earliest phase of star formation. Future IR studies may shed light on the nature of these objects.

Analysis of the FCRAO CO ^{12}CO and ^{13}CO data cubes obtained as part of the COMPLETE survey (Ridge et al. 2006) revealed the presence of some high velocity line wings similar to those produced by bipolar molecular outflows (Borkin 2006). Over a half-dozen such features were found. More detailed follow-up observations are needed to determine if these features are genuine outflow lobes, merely the signatures of intermittency in a turbulent flow, or unrelated features along the line of sight.

Interestingly, this portion of the Perseus cloud is superimposed on the diffuse HII region and IRAS dust ring, G159.6-18.5. It is possible that interaction with this ring has affected its global properties. The expansion of the ring may have recently compressed surrounding gas, leading to a phase transformation from atomic to molecular phases. Perhaps this dead-zone is the youngest portion of the Perseus molecular cloud, formed by the expansion of the dust ring. Such a picture might explain the relative lack of very young stars, outflows, and Herbig-Haro objects in this part of Perseus, the turbulent motions observed in the gas, and the presence of only some low-mass cloud cores observed with SCUBA and Bolocam.

4.5. Barnard 1

Barnard 1 (B1) lies approximately one degree east of NGC 1333 (Figure 3) in the center of the Perseus cloud. B1 is separated from NGC 1333 by a degree-scale cavity in the distribution of CO which can be seen in Figures 5 and 6. The mass of the B1 core is about 1200 $M_{\odot}$ (Bachiller & Cernicharo 1984; Ungerechts & Thaddeus 1987; Bachiller et al. 1990b). In the 850 μm SCUBA (Hatchell et al. 2005) and 1.1 mm Bolocam maps, the B1 cloud appears cometary with a tail facing directly away from the star 40 Per, one of the most massive main-sequence stars in the Per OB2 association.

The Barnard 1 cloud core is the first to have its line of sight magnetic field strength (27 ± 4 microgauss) measured by the Zeeman splitting of the OH molecule (Goodman et al. 1989). At the peak, the magnetic energy density is comparable to the kinetic energy density in turbulent motions, and the gravitational potential energy. Matthews & Wilson (2002) studied the polarization of submillimeter emission from the core of B1 which reveals the magnetic field orientation in the plane of the sky. They found evidence for an ordered magnetic field across the main core of B1 with a position angle (P.A.) of roughly 90° east of north. Of the four clumps in the core of B1 (B1-a, B1-b, B1-c, and B1-d following the nomenclature of Hirano et al. 1999), the two brightest (B1-b and B1-c) exhibit different mean P.A.s of polarization than the rest of the region.

B1 was initially thought to be a dark cloud in either pre-stellar, or possibly in the earliest stages of star formation. However, the IRAS satellite found several embedded infrared sources and YSOs (Ladd, Lada, & Myers 1993) in or near this dark cloud. Walawender et al. (2005b) identify at least 6 YSOs in B1 which drive outflows (LkHα 327, SMM 2, SMM 6, SMM 11, B1-bN, and B1-bS). Analysis of the SCUBA data reveals at least 12 clumps of dense dust. The Spitzer observations show that there is a small cluster of extremely young YSOs in B1.

The B1 region contains about a dozen 850 μm cloud cores, several IRAS sources, over a dozen Spitzer detected YSOs, and many HH objects and near-IR shocks. Alten et al. (1997) and Yan et al. (1998) found the first several HH objects, HH 429, 431, 432, and 433. The deep CCD survey of Walawender et al. (2005a) found another 18 shocks. Most of these shocks are faint and their morphology is unclear. However, several parsec-scale flows originate in the B1 region as discussed below. Walawender et al. (2008) found an additional 24 H_2 shocks that do not have HH object counterparts.

The source B1-IRS (B1-a, IRAS 03301+3057, or SMM6) is surrounded by a relatively large abundance of CCS emission, perhaps indicating the extreme youth of this protostar (De Gregorio-Monsalvo et al. 2005). These authors also find a cluster of 22 GHz water masers near this source. It was not, however, detected in X-rays by Yamauchi et al. (2001). A bipolar molecular outflow was first found in the vicinity of IRAS 03301+3057 by Nakayama (1988) and subsequently mapped by Hirano et al. (1997). This outflow contains strong thermal SiO emission which is usually associated with the youngest outflows. A string of H_2 knots emerges form IRAS 03301+3057 and may be associated with the CO flow detected by Hirano et al. (1997).

Near-IR H_2 images (Walawender et al. 2005b, 2008) reveal a spectacular bipolar H_2 flow consisting of features MH1 to the east, and MH2 to the west that emerges from the Class 0 protostar SMM2 (also known as B1-c) at PA $\sim$ 100/280°. The Spitzer space telescope band 2 (4.5 μm) images (Jørgensen et al. 2006) show that this flow is point-symmetric and S-shaped. Matthews et al. (2006) presented arcsecond resolution CO maps obtained with the BIMA millimeter-wave interferometer. The Spitzer images and CO maps of the outflow emerging from SMM2 / B1-c are shown in Figure 10. The shock structure revealed by the infrared images implies that the jet beam is precessing with a period short compared to the dynamical age of the most distant H_2 knots in this flow.

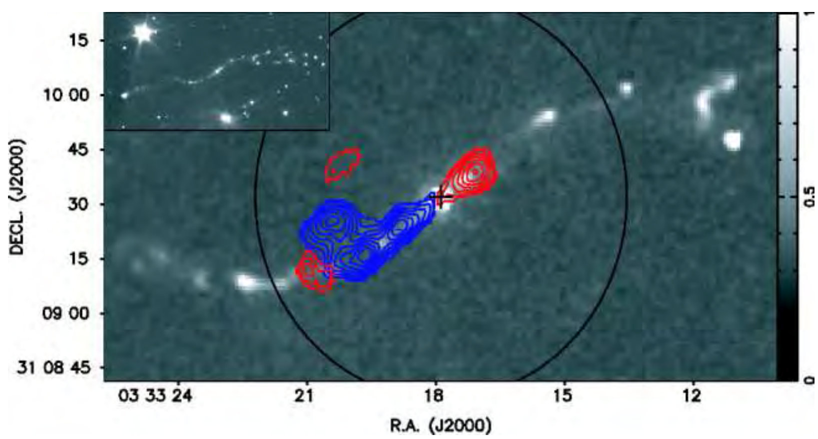

Figure 10. IRAC Spitzer data at 4.5 μm from Jørgensen et al. (2006) are compared to moment maps of the ^{12}CO J = 1 – 0 emission over the blue and red lobes of the bright H_2 outflow in the core of B1. The inset shows the larger scale extent of the molecular hydrogen emission with Spitzer. ^{12}CO J = 1 – 0 contours are from 3 – 10 Jy beam^{-1} km s^{-1}, in steps of 1 Jy beam^{-1} km s^{-1}. The large circle indicates the primary beam of a BIMA antenna. From Matthews et al. (2006).

The brightest source in the B1 region in the Spitzer IRAC images is IRAS 03304 +3100 (LkHα 327) located several arcminutes northeast of the B1 core. This star is visible at visual and near-IR wavelengths (m$_V$ = 14.9, m$_K$ = 7.7) and drives a large-scale outflow towards the southeast at PA $\sim$145° that includes HH 432, the H_2 shock MH 7 and HH 791, 793, and 794 located about 20 to 25′ to the southeast of the source

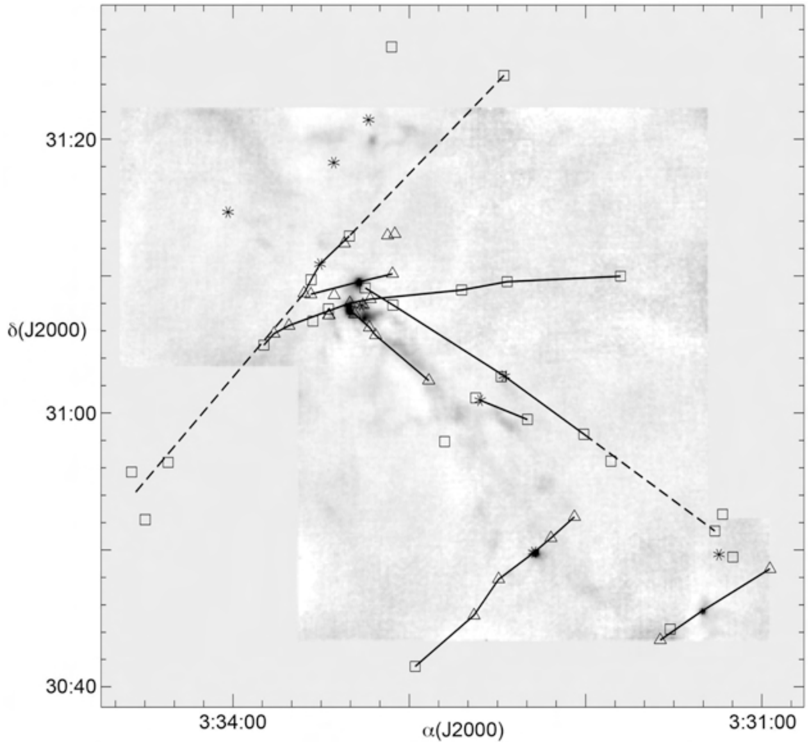

Figure 11. Gray-scale image of the 850 μm SCUBA map covering the B1 region. Squares and triangles represent HH objects and H_2 shocks, respectively. Asterisks represent IRAS sources. Taken from Walawender et al. (2008).

(Walawender et al. 2008). The latter three HH objects are the brightest portions of a 10′-scale bow shock whose orientation is consistent with being driven by a jet from IRAS 03304+3100. The projected length of the southeast lobe of this outflow is about 1.8 pc. HH 788 located a few arcminutes from the star towards the northwest may trace a counterflow. HH 430, located 20′ northwest of LkHα 327 may also be part of this giant outflow.

A parsec scale flow stretches from HH 433 on the east to HH 429 on the west (Walawender et al. 2008). This is linked by intermediate HH objects and H_2 shocks through the core of B1, though identification of the source protostar is uncertain due to the highly confused nature of the overlapping outflows in the core of B1.

Additional YSOs can be found at the periphery of B1 (Figure 11). To the north, there are two IRAS sources, IRAS 03301+3111 and IRAS 02203+3108, a sub-mm core, SMM10, and several HH objects, HH 430 and HH 356. Several YSOs and outflows are also located southwest of B1. These include IRAS 03293+3052 which is associated with a compact H_2 bow shock and HH object HH 783 and IRAS 03295+3050 associated with a prominent C-shaped reflection nebula and jet in H_2 images. IRAS 03293+3052 appears to drive a long flow which stretches from the core of B1 (the HH 431 and 787 shocks) to the HH 770-772 shocks which lie over 30′ to the southwest.

The profusion of HH objects and near-IR shocks, the presence of several parsec-scale outflows, and over a dozen YSOs, many of which are seen at visual wavelengths demonstrates that the B1 region has been an active site of star formation for quite some time.

4.6. The Bridge Connecting B1 to L1455

A ridge of molecular gas bridges the region between B1 and L1455 (see Fig. 6). This feature traces the southern rim of a degree-scale V-shaped cavity located between B1 and NGC 1333 that opens towards north by northeast. The chain of cloud cores in this ridge contain sub-mm cores, IRAS sources, outflows, and HH objects, indicating extensive star formation in this region.

Starting from B1, the cores SMM5 and SMM7, located $25' - 30'$ southwest of B1-IRS, contain IRAS 03292+3039 and IRAS 03282+3035. Walawender et al. (2005a) postulated that HH 782, a $10'$ long filament of [SII] emission extending southeast from IRAS 03292+3039 and ending in a bright but compact bow shock, traces a shock in a flow from IRAS 03292+3039 (Fig. 12). The Spitzer IRAC (c2d) survey confirms this suggestion by the detection of a spectacular highly collimated, $25'$ long, bipolar parsec-scale outflow most visible in IRAC Band 2 (centered on 4.5 μm) that emerges from the IRAS source along a northwest–southeast direction (PA $\sim$ 150/330°). The IRAC images reveal a small, conical reflection nebula facing southeast, suggesting that HH 782 traces the blue-shifted lobe of this outflow. The IRAS 03292+3039 flow consists of a chain of bow shocks and exhibits gentle bends, possibly indicating that the flow-ejection direction has changed with time.

IRAS 03282+3035 is a young star as evidenced by X-ray emission detected by Yamauchi et al. (2001). It is embedded in the submillimeter core SMM7 and is associated with HH 773. The parent cloud core is illuminated from the northeast and in visual wavelength images exhibits a cometary morphology suggesting that it has been shaped by radiation from a source located to the northeast. The highly collimated bipolar molecular outflow from this Class 0 source was one of the first to exhibit high-velocity 'bullets' of CO emission (Bachiller, Martin-Pintado, & Planesas 1991). Aspin (1992), Bally et al. (1993a), and Bachiller et al. (1994) detected shock-excited H_2 emission from the southeast (blueshifted) lobe of this outflow. Subsequent studies probed the dense core containing the IRAS source and the shear where the molecular jet interacts with surrounding medium (Tafalla et al. 1993; Bachiller et al. 1994). The Spitzer c2d survey shows that this flow is bipolar and at least $10'$ in length with an orientation similar to the giant flow from IRAS 03292+3039 (PA $\sim$ 140/310^o). Gentle S-shaped bending may indicate an orientation-variable outflow.

The large IRAS 03292+3039 and IRAS 03282+3035 outflows are nearly parallel to each other, and emerge orthogonal to the filament of dust and molecular gas between Barnard 1 and L1455 (Figure 12).

In a recent analysis of Spitzer 24, 70, and 160 μm MIPS scan-maps, Rebull et al. (2007) present mid-IR observations of a new aggregate of embedded protostars located about $18'$ farther southwest along the CO ridge extending from B1 to L1455. This region, previously dubbed Per 6 in the NH_3 study of Ladd et al. (2004), contains 10 MIPS-detected mid-IR objects located within a $11'$ x $2.5'$ region. Four are IRAS sources, including IRAS 03271+3013, IRAS 03273+3018, IRAS 03275+3020, and IRAS 03276+3022 (LkHα 326). This cluster of YSOs is elongated along the orientation of the ridge of molecular gas and dust connecting B1 to L1455. Per 6 contains several sub-mm and mm-bright cores (Enoch et al. 2006; Kirk et al. 2006), and CS cores (Hatchell et al. 2005). Several HH objects cluster around this region (Yan et al.

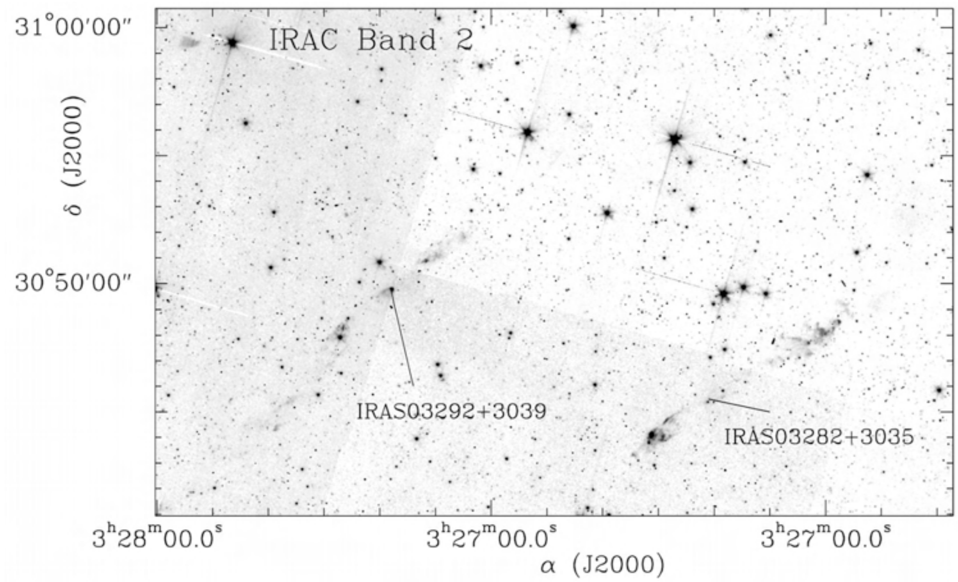

Figure 12. The nearly parallel IRAS 03292+3039 (left) and IRAS 03282+3035 (right) outflows in the bridge between B1 and L1455 as seen in the Spitzer 4.6μm images. The lower-left (southeast) portion of the IRAS 03292+3039 outflow is known as HH 782 (Walawender et al. 2005a). (Courtesy of the c2d team).

1998; Walawender et al. 2005a - see their Figure 26). This region contains a pair of fairly bright reflection nebulae. Aspin (1992) detected a bipolar high-velocity molecular outflow from the brightest YSO, IRAS 03271+3013 (also see Wu et al. 2004). The presence of four IRAS and 10 MIPS-detected mid-IR sources, CO outflows, multiple reflection nebulae, and the cluster of HH objects indicates that extensive star formation has occurred recently in this region.

4.7. NGC 1333

NGC 1333 is currently the most active region of star formation in the Perseus molecular cloud. The NGC 1333 region is discussed in detail in the chapter by Walawender et al. in this Handbook. The presence of emission-line stars and Herbig-Haro objects first established NGC 1333 as an active region of star formation (Herbig & Rao 1972; Herbig 1974). NGC 1333 is one of the best studied extremely young clusters of low to intermediate mass stars, and one of the most active sites of ongoing star formation in the sky within 500 pc of the Sun (Lada, Alves & Lada 1996). This region is rich in sub-mm cores (Hatchell et al. 2005; Enoch et al. 2006; Kirk et al. 2006), embedded YSOs (Aspin, Sandell, & Russell 1994 ; Jørgensen et al. 2006), radio continuum sources (Rodríguez, Anglada, & Curiel 1999), masers (Rodríguez et al. 2002 ; Furuya et al. 2003), IRAS sources, SiO molecular jets (Choi 2005), H_2 and HH shocks (Bally, Devine, & Reipurth 1996), and molecular outflows (Knee & Sandell 2000), and the lobes of extinct outflows (Quillen et al. 2005). Dozens of outflows from embedded and young cluster members criss-cross this region. While the complexity and confusion of sources and outflows has made it difficult to unravel the relations between various components, NGC 1333 has illuminated the roles of feedback and clustering phenomena in star formation (e.g. Walawender et al. 2005a).

The Ridge South of NGC 1333 The molecular ridge extending south from NGC 1333 to the L1455 region contains many HH objects and IRAS sources. HH 14, the brightest and most complex shock in this region, is located about 20′ south of NGC 1333. The survey of Walawender et al. (2005a) shows many fainter shocks.

NGC 1333 and the regions extending about 1 degree south contains an extensive network of filamentary visual wavelength and near-infrared nebulae consisting of jets, chains of irregular shocks, and bow shocks. The complex Herbig-Haro object HH 14 is the brightest feature south of NGC 1333. Although its morphology might indicate motion towards the northeast, proper motions indicate that it is moving nearly due south along the roughly north-south oriented molecular ridge which connects NGC 1333 to L1455. HH 351 is a large, but faint complex of visual-wavelength knots, bow shocks, and filaments scattered over a several arcminute-wide region south by southwest of HH 14. There is a giant H_2 bow shock, evident in both ground-based and Spitzer data, about 30′ south-southwest of HH 14. This feature appears to mark the southern end of the profuse outflow activity and shocks which permeate the molecular ridge south of the NGC 1333 cluster.

4.8. L1455 and L1451

L1455 is located near the southwest end of the Perseus cloud (Figures 3, 4, 5, and 6) about 70′ south and slightly west of NGC 1333 and about 40′ southeast of L1448. L1455 and the nearby L1451 region contains six previously known objects (HH 279, 280, 317, 318, 422, and 423) and four recently discovered objects: HH 492, 493, 739, and 743 (Walawender et al. 2004). The L1455 core has a mass of 40-50 $M_\odot$ (Bachiller & Cernicharo 1986b). It contains three known YSOs (Bally et al. 1997). Bally et al. (1997) found that the association of a particular HH object with a particular YSO in both L1448 and L1455 was difficult, because many of the HH objects are a parsec or more from the nearest source. They suggest that outflows from one cloud may actually interact with the other, thus an outflow source in one cloud may generate shocks and inject energy into the adjacent cloud.

The visually most conspicuous source in L1455 is IRAS 03247+3001 (L1455 IRS 2) associated with a red reflection nebula, RNO 15. The nebula consists of a fan of light which opens towards the south of the infrared source. However, this source drives a CO outflow towards the northwest and southeast (Goldsmith et al. 1984; Levreault 1988) consistent with the giant outflow shown in Figure 13.

Bally et al. (1997) discovered a large arcminute-scale and very bright HH object, HH 279, located about 8′ northwest of RNO 15. The Spitzer IRAC 4.5μm images (Figure 13) show a highly collimated giant outflow centered on RNO 15 with an axis having orientation PA $\sim$ 135/315°. HH 279, located along the northwest portion of this flow marks the location of the brightest shock complex in the IRAC 4.5μm images. Nearly continuous emission can be traced from HH 279 back to RNO 15. A faint, but continuous filament of sinuous emission extends southeast of RNO 15 towards a bright, oblique bow shock located on the bottom left of Figure 13.

A deeply embedded infrared source, IRAS 03245+3002 (L1455 IRS 1) is located about 2′ northwest of RNO 15. Davis et al. (1997a,b) present deep near-IR imaging and CO maps of the outflows emerging from L1455 IRS 1 and its vicinity. They find an

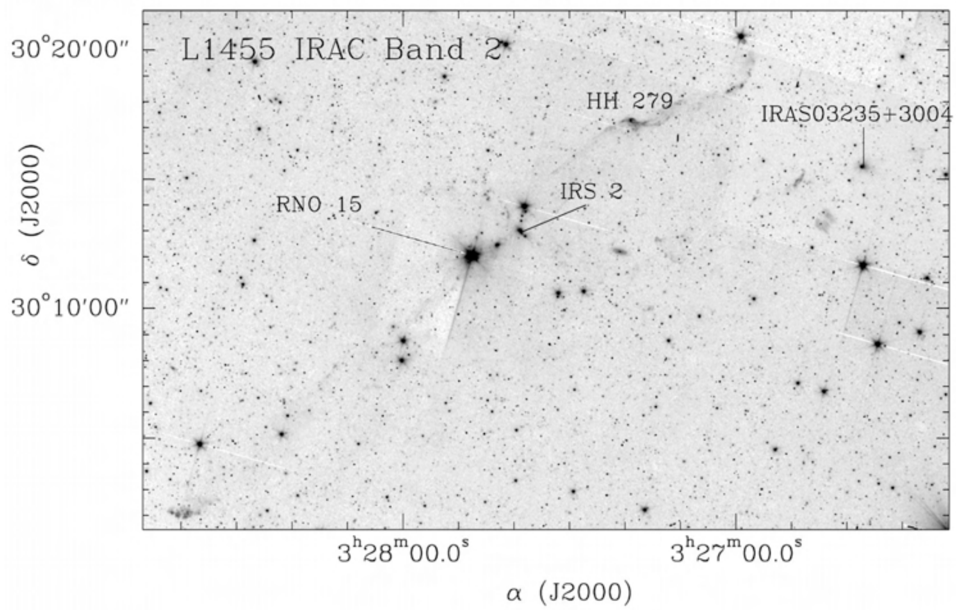

Figure 13. The parsec-scale outflow emerging from RNO 15 (centered; this is source #8 in Table 1) embedded in the L1455 cloud core in a Spitzer IRAC Band 2 image showing the emission at 4.5 μm. The bright shock complex in the upper-right is HH 279, the brightest shock in the L1455 region. While RNO 15 drives a large southeast–northwest flow, IRAS 03247+3001 drives a much smaller flow oriented northeast–southwest. IRAS 03235+3004 is the source a a giant flow containing HH 280 west of the source, and HH 492, 493, and 317 east of the source (Figure 14 shows a visual wavelength images of this flow). Note the similar orientations of the outflows from IRAS 03292+3039, IRAS 03282+3035, and RNO 15. (courtesy of the c2d team).

HH object about 35″ due south of RNO 15, and a number of HH objects (labeled B, C, D, and E in Davis et al. 1997a) located northeast of L1455 IRS 1. This latter group of HH objects are associated with the red-shifted lobe of a highly collimated CO outflow emerging from L1455 IRS 1 towards PA $\sim$ 40/220°. These HH objects are also visible in the 2.12 μm S(1) line of H_2. Interestingly, the Davis et al. (1997a) data shows a compact and faint HH knot northwest of both RNO 15 and L1455 IRS 1.

Deep images of the region located about 20′ west of L1455 reveal an additional parsec-scale flow bursting out of a cometary shaped cloud located 6.3′ northeast of the L1451 cloud core and 19.5′ west of the L1455 cloud core (Figure 14). This giant outflow is composed of HH 280, 317, 492, and 493 and is described in detail in Walawender et al. (2004). This flow is driven by IRAS 03235+3004, which is embedded in the tip of the cometary cloud near a line drawn between HH 493 and HH 280. The IRAS source has been previously investigated by Ladd, Lada, & Myers (1993) who find it to be a low-luminosity Class-I source. The IRAS source is surrounded by a dense cloud core and may be accreting material; Gregersen et. al. (2000) found a self-reversed HCO^+ emission-line profile and Mardones et. al. (1997) detected low-velocity redshifted line wings in CS and H_2CO.

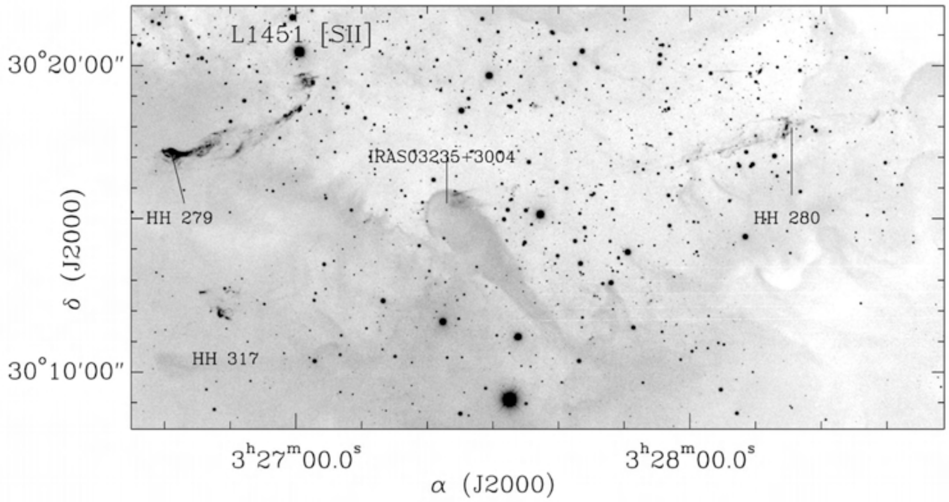

Figure 14. A KPNO 4 meter prime-focus Mosaic CCD image showing [SII] emission from the HH 280 outflow emerging from the cometary L1451 cloud that points towards the early-type star 40 Per. HH 279 associated with the RNO 15 outflow is located in the upper-left portion of this image. HH 317 may trace the counterflow from IRAS 03235+3004 (Walawender et al. 2005).

Walawender et al. (2004) suggest that this cometary cloud is sculpted by a soft UV source lying somewhere along its axis. Two bright early-type stars lie close to a line drawn along the axis of the cometary cloud: the 4^{th} magnitude O7e star ξ Persei, which illuminates the California Nebula (NGC 1499), and the 5^{th} magnitude B0.5V star 40 Persei. The cometary cloud points to within ten degrees of ξ Persei and within three degrees of 40 Persei. Thus, the latter star is a strong candidate for illuminating the cometary cloud. Its Hipparcos parallax, 3.53 ± 0.88 mas, places it at a distance of 283^{+94}_{-56} pc, and it is listed as a member of the Per OB2 association (de Zeeuw et al. 1999). The separation between the cometary cloud and 40 Per is 299′, or 26 pc in projection, assuming a distance of 300 pc.

The identification of 40 Persei as the illuminating source is supported by the work of Kirk et al. (2006) who used offsets between submillimeter clumps and ^{13}CO cores as a vector indicating the direction of an external triggering source. The vectors in Perseus all point toward the center of the Per OB2 association in general and 40 Persei in particular (see Kirk et al. 2006 Figure 10).

4.9. L1448

L1448 at the west end of the Perseus cloud has a total molecular mass of approximately 100 $M_\odot$ concentrated in two dense cores of about 50 $M_\odot$ each (Bachiller & Cernicharo 1986a, b; Wolf-Chase et al. 2000). L1448 contains a half dozen YSOs (O'Linger et al. 2006) that drive molecular outflows and chains of HH objects (Wolf-Chase, Barsony, & O'Linger 2000; Bally et al. 1997; Walawender et al. 2005). IRAS detected three sources in this region (Bachiller & Cernicharo 1986a). IRAS 03220+3035, also known as L1448 IRS1, has a visual counterpart with m_V = 19.5 mag (Cohen & Kuhi 1979) and is associated with the visual-wavelength reflection nebula RNO 13. Thus this source is a Class II YSO. IRAS 03222+3034 (L1448 IRS 2) is a highly embedded Class 0 protostar

(O'Linger et al. 1999). IRAS 03225+3034, also known as IRS 3, is an embedded Class 0/I source that has three components, A, B and C (Looney et al. 2000; Kwon et al. 2006).

The most magnificent feature in L1448 is the highly collimated, C-symmetric CO outflow first mapped by Bachiller et al. (1990a) and originating from a location south of IRS3 where no IRAS source was detected. Following the discovery of the outflow, a protostar was found at the point of symmetry at millimeter and centimeter wavelengths (Bachiller et al. 1991; Curiel et al. 1990) and is referred to as L1448-mm or L1448-C(enter). Barsony et al. (1998) measured the spectral energy distribution from far-infrared to millimeter wavelengths and established the Class 0 status of L1448-C.

Bally, Lada, & Lane (1993), Davis et al. (1994), and Davis & Smith (1995) mapped the shock-excited H_2 emission from the L1448-C outflow, finding it to be one of the highest velocity, best collimated, and youngest outflows known at the time. High-resolution CO maps obtained with the IRAM interferometer demonstrated that the CO emission was confined to shells of expanding gas surrounding relatively evacuated cavities that contained high velocity, predominantly molecular jets (Bachiller et al. 1995). Guilloteau et al. (1992) obtained $2''$ resolution maps of SiO emission from these jets, finding them to have densities of order n(H_2) $\approx 10^7$ cm^{-3}. The abundance of SiO in these jets was found to be enhanced by a factor of order 10^5 or more compared to the quiescent molecular gas in the host cloud. These and the subsequent high-resolution SiO images of Dutrey et al. (1997) clearly demonstrated that the outflow was powered by an episodic and highly collimated jet consisting primarily of molecular gas and that this jet inflated cavities surrounded by shock-excited H_2 emission and swept-up CO emitting gas.

Davis et al. (1995) found that the multiple star system IRS3, located less than $1'$ north of L1448C, drives a separate outflow parallel to the L1448C outflow. Recent studies have shown that each component of this triple star system powers an outflow. At least one of these flows has reached parsec-scale dimensions.

Wolf-Chase et al. (2000) found that outflows within L1448 contain between 16 and 24 $M_\odot$ km s^{-1} of momentum which is nearly equivalent to the momentum content of the quiescent cores. In addition, the energy content of the outflows ($2 - 8 \times 10^{45}$ ergs) exceeds the gravitational binding energy of the entire 100 $M_\odot$ L1448 complex ($\mathrm{GM}^2/\mathrm{R} \approx 5 \times 10^{44}$ ergs). Thus Wolf-Chase et al. (2000) conclude that L1448 is likely to be dispersed by protostellar outflows.

Tsujimoto, Kobayashi, & Tsuboi (2005) conducted deep X-ray and IR observations of the L1448 cloud and identified ten additional YSOs and candidate brown dwarf stars brighter than m_K = 17. This study also may have detected X-rays from L1448 IRS3(A), making it the most embedded Class 0 / I protostar to exhibit X-ray emission.

Bally et al. (1997) obtained wide-field narrow-band images covering over a square degree. They found many Herbig-Haro objects surrounding the L1448 dark cloud. Chains of these HH objects are aligned with the outflow axes of the L1448C and IRS3 outflows. Additionally, shocks were seen along an axis passing through the Class 0 source, IRS2, and which appears to emerge from the vicinity of the reflection nebula RNO 13. Wolf-Chase et al. (2000) mapped a large region surrounding L1448 in CO and found that parsec-scale CO outflows are powered by L1448C, IRS2, and IRS3 along the axes of the HH flows. Deep, wide-field, near-IR images of H_2 by Eislöffel (2000) confirmed the connection between the dense molecular jets, CO outflows, and chains of HH objects in the vicinity of the L1448 cloud.

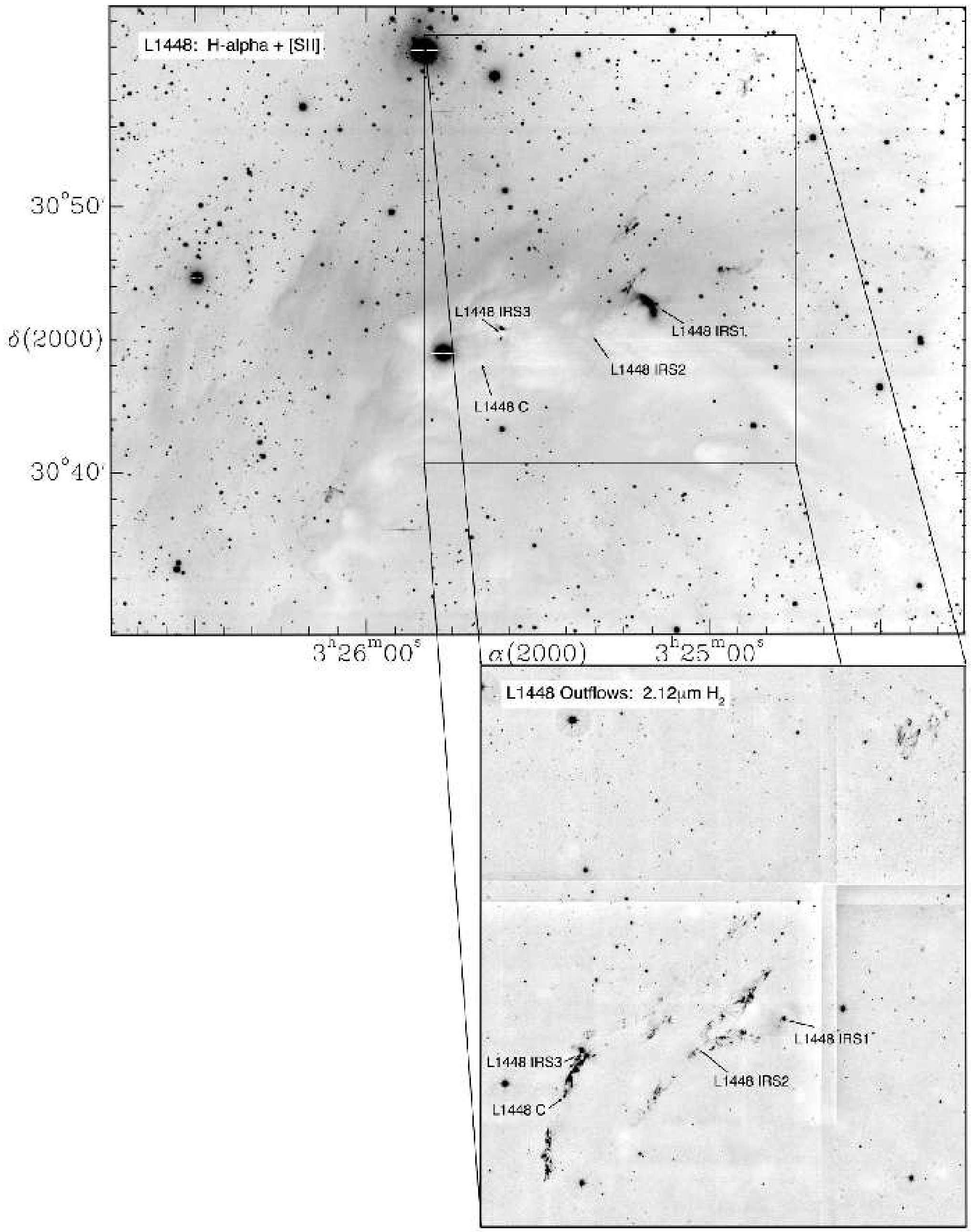

Figure 15. The L1448 region in Hα + [SII] observed with the prime focus Mosaic CCD on the Mayall 4 meter (top), and 2.12 μm H_2 observed with WFCAM on UKIRT (bottom). L1448-C drives the brightest 2.12 μm outflow seen in the WFCAM image. IRS 3 drives a parsec scale flow whose southeastern lobe is shown in Figure 16. Several shocks found by Bally et al. (1997) towards the northwest are also likely powered by IRS 3. The more evolved YSO, IRS 1 appears to illuminate the reflection nebula RNO 13 and drives a nearly east–west flow. The Class 0 source IRS 2 drives a flow nearly parallel to the giant flow powered by IRS 3.

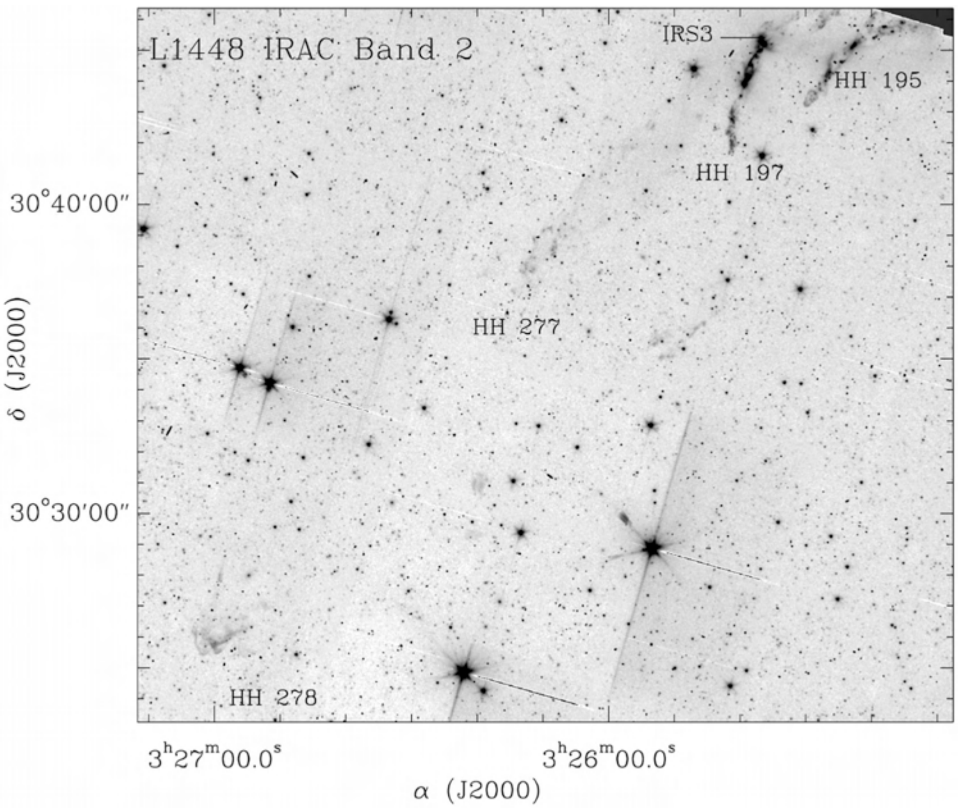

Figure 16. An IRAC Band 2 (4.5 μm) image taken with the Spitzer Space Telescope showing the region between L1448 (upper right) and L1455 (off this frame towards the lower left). One component of IRS 3 appears to drive a parsec scale outflow that extends towards the southeast and contains HH 277 and 278. These compact HH objects are surrounded by a nearly continuous sheath of emission (presumably produced by shock-excited H_2) that connects this outflow to the IRS3 region. HH 197 is the only portion of the outflow from L1448-C that is visible at visual wavelengths. Yet, in the near-IR, the L1448-C flow is the brightest and most spectacular outflow in this region. Thus, most of its shocks must be hidden by lots of extinction. HH 195 is the visual wavelength counterpart of a giant flow powered by IRS 2. These outflows can also be seen in the WFCAM image shown in Figure 15. Image courtesy c2d team.

The Spitzer IRAC 4.5μm images show that several of the outflows emerging from L1448 extend towards and nearly reach the L1455 cloud located to the southeast (Figures 15 and 16). The largest flow emerges from one of the components of IRS3 towards the southeast and contains HH 277 and 278. The HH 195 flow emerging from IRS 2 and the spectacular H_2 flow from L1448-C are also evident in this figure. It is remarkable that at least three of the L1448 outflows, L1448-C, IRS2, and IRS3, have southeast–northwest orientations having a position angle of approximately PA $\sim$ 135 / 315°, similar to the orientations of the three large Spitzer-detected flows emerging from RNO 15 in L1455, and IRAS 03282+3035 and IRAS 03292+3039 in the southern portion of Perseus in the ridge connecting L1455 to B1.

5. Conclusions

The Perseus molecular cloud is the closest available laboratory for the investigation of low to intermediate mass star formation in a moderate mass giant molecular cloud giving birth to both clusters and relatively isolated stars. The Perseus cloud appears to be in the interior or possibly the periphery of a small supershell blown into the surrounding ISM by the Per OB2 association. Although the GMC is not currently forming massive stars, some high-mass star formation giving rise to stars more massive than about 10 $M_{\odot}$ has occurred in the recent past as evidenced by the presence of the low-surface brightness HII region G159.6-18.5 that is in direct contact with the northeastern part of the molecular cloud. The young clusters IC 348 and NGC 1333 have given birth to several moderate-mass late B-type stars in the recent past.

Spitzer Space Telescope observations have led to the identification of over 400 Class I and II YSOs. Additionally, the cloud contains many highly embedded Class 0 sources best identified as the highly obscured denizens of the sub-mm / mm cloud cores identified by the SCUBA 850 μm and Bolocam 1.1 mm dust continuum surveys. Some of these Class 0 sources, such as L1448 C, were first identified by their outflows.

The combination of ground-based CCD near-IR imaging surveys with narrow-band filters, the Spitzer / IRAC campaigns, and mapping of the high-velocity wings of CO and other millimeter (and sub-millimeter) transitions has led to the discovery of dozens of outflows from the Perseus YSOs. Many have attained parsec-scale dimensions, and are making a substantial contribution to the gas dynamics and turbulent energy budgets of their host cloud cores.

The Perseus molecular cloud, its population of YSOs and outflows provide us with the most complete view of the ”ecology” of star formation over an entire GMC. However, many questions remain to be answered. What is the exact relationship between the Per OB2 association and the GMC? Why are there significant radial velocity differences between the Per OB2 stars and the GMC? What causes the large, nearly 10 km s^{-1} velocity gradient from the east to the west end of the cloud? Was the formation of the two clusters, IC 348 and NGC 1333, triggered? Is the current burst of star formation in the ”Flying Ghost Nebula”/ HH211 region southwest of IC 348 being triggered by IC 348 itself? What is the dominant source of illumination of the cloud surfaces in Perseus? Why are many of the outflows in the ridge between B1 and L1455 and in L1448 nearly parallel to each other? Why is there a large degree-scale cavity between NGC 1333, Barnard 1, and L1455? Is there a loose cluster of young stars inside this cavity? What is the total young star population of the Perseus OB2 region? How many Class III and post T-Tauri but pre-main sequence stars are there in this complex?

Answers to these questions will require large-scale surveys. Future studies might include:

- Deep X-ray surveys to identify Class III and weak-line T-Tauri stars by means of their flaring X-ray emission.
- Synoptic monitoring of visual wavelength stars down to at least m_V = 18 mag. so as to reach the boundary between M stars and brown dwarfs to identify young, pre-main sequence candidates by means of their irregular variability.
- A program of multi-object spectroscopy to identify pre-main sequence stars by means of their Hα emission, lithium absorption, and other spectral signatures of youth.
- A program of multi-object high resolution spectroscopy to measure the radial velocities of stars to about 1 km s^{-1} to establish membership, to resolve and establish moving groups, and to identify spectroscopic multiples.

• A campaign to search for water and methanol masers among the embedded YSOs that can be used for precision parallax measurements with the VLBA to establish a network of fiducial reference points whose distances are known to a few percent.

• Continued high-resolution interferometric studies with CARMA, SMA, VLA, and eventually ALMA to investigate circumstellar disks, jets, and outflows. Perseus offers some of the nearest sources for the detailed investigation of low to moderate mass YSOs. It is the closest cloud where sufficient numbers of sources in various evolutionary stages are available for meaningful statistical investigations.

Acknowledgments. We acknowledge support by NASA grant NNA04CC11A to the CU Center for Astrobiology and NSF grant AST0407356. JW was supported by the NSF through grants AST-0507784 and AST-0407005. We thank the COMPLETE team for their contributions. This research has made use of the SIMBAD database, operated at CDS, Strasbourg, France. This research has made use of NASA's Astrophysics Data System. We also thank Adam Block and Jeff Lunglhofer for their contributions of Figures 3 and 4, respectively.

References

Arce, H. G., Goodman, A. A., Bastien, P., Manset, N., & Sumner, M. 1998, ApJ, 499, L93
Alten, V. P., Bally, J., Devine, D., & Miller, G. J. 1997, IAU Symp. 182 Poster Book *Low Mass Star Formation – from Infall to Outflow*, eds. Malbet, F., & Castets, A., p.51
Andersson, B.-G., Wannier, P. G., Moriarty-Schieven, G. H., & Bakker, E. J. 2000, AJ, 119, 1325
Aspin, C. 1992, A&A, 266, 416
Aspin, C., Sandell, G., & Russell, A. P. G. 1994, A&AS, 106, 165
Avila, R., Rodríguez, L. F., & Curiel, S. 2001, Rev. Mex. Astron. Astrofis. 37, 201
Bachiller, R. & Cernicharo, J. 1984, A&A, 140, 414
Bachiller, R. & Cernicharo, J. 1986a, A&A, 168, 262
Bachiller, R., & Cernicharo, J. 1986b, A&A, 166, 283
Bachiller, R., Martin-Pintado, J., Tafalla, M., Cernicharo, J., & Lazareff, B. 1990a, A&A, 231, 174
Bachiller, R., del Rio Alvarez, S., & Menten, K. M. 1990b, A&A, 236, 461
Bachiller, R., Martin-Pintado, J., & Planesas, P. 1991, A&A, 251, 639
Bachiller, R., Andre, P., & Cabrit, S. 1991, A&A, 241, L43
Bachiller, R., Terebey, S., Jarrett, T., Martin-Pintado, J., Beichman, C.A., & Van Buren, D. 1994, ApJ, 437, 296
Bachiller, R., Guilloteau, S., Dutrey, A., Planesas, P., & Martin-Pintado, J. 1995, A&A, 299, 857
Bally, J. 2001, ASP Conf. Ser. 231 *Tetons 4: Galactic Structure, Stars and the Interstellar Medium*, 231, 204
Bally J., Devine D., Hereld M., & Rauscher B.J. 1993a, ApJ, 418, L75
Bally J., Lada C.J., & Lane, A.P. 1993b, ApJ, 418, 322
Bally, J., Devine, D., & Alten, V. 1996, ApJ, 473, 921
Bally, J., Devine, D., & Reipurth, B. 1996, ApJ, 473, L49
Bally, J., Devine, D., Alten, V., & Sutherland, R. S. 1997, ApJ, 478, 603
Barnard, E. E. 1913, ApJ, 38, 496
Barnard, E. E. 1919, ApJ, 49, 1
Barsony, M., Ward-Thompson, D., André, P., & O'Linger, J. 1998, ApJ, 509, 733
Basu, S. & Murali, C. 2001, ApJ, 551, 743
Beichman, C. A., Jennings, R. E., Emerson, J. P., Baud, B., Harris, S. et al. 1984, ApJ, 278, L45
Beichman C.A., Wilson R.W., Langer W.D., & Goldsmith P.F. 1988, ApJ, 332, L81

Belikov, A. N., Kharchenko, N. V., Piskunov, A. E., Schilbach, E., & Scholz, R.-D. 2002, A&A, 387, 117
Bhatt, H. C. 1986, MNRAS, 222, 383
Blaauw, A. 1952, Bull. Astron. Inst. Neth., 11, 405
Blaauw, A. 1964, ARA&A, 2, 213
Blaauw, A. 1991, NATO ASIC Proc. 342: *The Physics of Star Formation and Early Stellar Evolution*, edited by Lada, C. J. & Kylafis, N. D., publisher: Kluwer 125
Borgman, J., & Blaauw, A. 1964, Bull. Astron. Inst. Neth., 17, 358
Borkin, M. A. 2006, Senior thesis, Harvard University http://www.cfa.harvard.edu/COMPLETE/papers/borkin.pdf
Boulard, M.-H., Caux, E., Monin, J.-L., Nadeau, D., & Rowlands, N. 1995, A&A, 300, 276
Černis, K. 1990, Ap&SS, 166, 315
Černis, K. 1993, Baltic Astronomy, 2, 214
Černis, K. & Straižys, V. 2003, Baltic Astronomy, 12, 301
Chandler, C. J. & Richer, J. S. 2001, ApJ, 555, 139
Choi, M. 2005, ApJ, 630, 976
Cohen, M. & Kuhi, L. V. 1979, ApJS, 41, 743
Curiel, S., Raymond, J. C., Moran, J. M., Rodríguez, L. F., & Canto, J. 1990, ApJ, 365, L85
Dame, T. M., Ungerechts, H., Cohen, R. S., de Geus, E. J., Grenier, I. A., et al. 1987, ApJ, 322, 706
Dame, T. M., Hartmann, D., & Thaddeus, P. 2001, ApJ, 547, 792
Davis, C. J., Dent, W. R. F., Matthews, H. E., Aspin, C., & Lightfoot, J. F. 1994, MNRAS, 266, 933
Davis, C. J. & Smith, M. D. 1995, ApJ, 443, L41
Davis, C. J., Mundt, R., Eislöffel, J., & Ray, T. P. 1995, AJ, 110, 766
Davis, C. J., Eislöffel, J., Ray, T. P., & Jenness, T. 1997a, A&A, 324, 1013
Davis, C. J., Ray, T. P., Eislöffel, J., & Corcoran, D. 1997b, A&A, 324, 263
de Zeeuw, P. T., Hoogerwerf, R., de Bruijne, J. H. J., Brown, A. G. A., & Blaauw, A. 1999, AJ, 117, 354
De Gregorio-Monsalvo, I., Chandler, C. J., Gómez, J. F., Kuiper, T. B. H., Torrelles, J. M., & Anglada, G. 2005, ApJ, 628, 789
Draine, B. T. & Lazarian, A. 1998, ApJ, 508, 157
Draine, B. T. & Lazarian, A. 1999, ApJ, 512, 740
Dutrey, A., Guilloteau, S., & Bachiller, R. 1997, A&A, 325, 758
Eislöffel, J. 2000, A&A, 354, 236
Eislöffel, J., Froebrich, D., Stanke, T., & McCaughrean, M. J. 2003, ApJ, 595, 259
Enoch, M. L., Young, K. E., Glenn, J., Evans, N. J., Golwala, S., et al. 2006, ApJ, 638, 293
Finkbeiner, D. P. 2003, ApJS, 146, 407
Fuller G. A., Myers P. C., Welch W. J., Goldsmith P. F., Langer W. D., et al. 1991, ApJ, 376, 135
Furuya, R. S., Kitamura, Y., Wootten, A., Claussen, M. J., & Kawabe, R. 2003, ApJS, 144, 71
Goldsmith, P. F., Snell, R. L., Hemeon-Heyer, M., & Langer, W. D. 1984, ApJ, 286, 599
Goldsmith P. F., Langer W. D., & Wilson R. W. 1986, ApJ, 303, L11
Goodman, A. A., Crutcher, R. M., Heiles, C., Myers, P. C., & Troland, T. H. 1989, ApJ, 338, L61
Goodman, A. A., Bastien, P., Myers, P. C., & Menard, F. 1990, ApJ, 359, 363
Gregersen, E. M., Evans, N. J., II, Mardones, D., & Myers, P. C. 2000, ApJ, 533, 440
Guilloteau, S., Bachiller, R., Fuente, A., & Lucas, R. 1992, A&A, 265, L49
Gueth, F. & Guilloteau, S. 1999, A&A, 343, 571
Hartmann, D. & Burton, W. B. 1997, *Atlas of Galactic Neutral Hydrogen*, Cambridge University Press
Hatchell, J., Richer, J. S., Fuller, G. A., Qualtrough, C. J., Ladd, E. F., & Chandler, C. J. 2005, A&A, 440, 151
Hatchell, J., Fuller, G. A., Richer, J. S., Harries, T. J., & Ladd, E. F. 2007a, A&A, 468, 1009
Hatchell, J., Fuller, G. A., & Richer, J. S. 2007b, A&A, 472, 187

Hatchell, J., & Fuller, G. A. 2008, A&A, 482, 855
Heiles, C. 1984, ApJS, 55, 585
Herbig, G. H. 1974, Lick Obs. Bull., No. 658
Herbig, G. H. 1998, ApJ, 497, 736
Herbig, G. & Rao, N. 1972, ApJ, 174, 401
Herbig, G. H. & Jones, B. F. 1983, AJ, 88, 1040
Herbig, G. H., Andrews, S. M., & Dahm, S. E. 2004, AJ, 128, 1233
Herbertz, R., Ungerechts, H., & Winnewisser, G. 1991, A&A, 249, 483
Hirano, N., Kameya, O., Mikami, H., Saito, S., Umemoto, T., & Yamamoto, S. 1997, ApJ, 478, 631
Hirano, N., Kamazaki, T., Mikami, H., Ohashi, N., & Umemoto, T. 1999, *Star Formation 1999*, Editor: T. Nakamoto, Nobeyama Radio Observatory, p. 181-182
Hirota T., Bushimata T., Choi Y. K., Honma M., Imai H., et al., 2008, PASJ, 60, 37
Jørgensen, J. K., Harvey, P. M., Evans, N. J., Huard, T. L., Allen, L. E., et al. 2006, ApJ, 645, 1246
Jørgensen, J. K., Johnstone, D., Kirk, H., & Myers, P. C. 2007, ApJ, 656, 293
Kirk, H., Johnstone, D., Di Francesco, J. 2006, ApJ, 646, 1009
Kirk, H., Johnstone, D., & Tafalla, M. 2007, ApJ, 668, 1042
Knee, L. B. G. & Sandell, G. 2000, A&A, 361, 671
Kwon, W., Looney, L. W., Crutcher, R. M., & Kirk, J. M. 2006, ApJ, 653, 1358
Lada, C. J., Alves, J., & Lada, E. A. 1996, AJ, 111, 1964
Lada, C.J. & Lada, E. A. 2003, ARA&A, 41, 57
Ladd, E. F., Lada, E. A., & Myers, P. C. 1993, ApJ, 410, 168
Ladd, E., Myers, P., & Goodman, A. 1994, ApJ, 433, 117
Langer, W. D., Wilson, R. W., Goldsmith, P. F., & Beichman, C. A. 1989, ApJ, 337, 355
Langer, W.D., Velusamy T., & Xie, T. 1996, ApJ, 468, L41
Levreault, R.M. 1988, ApJS, 67, 283
Lodieu, N., McCaughrean, M. J., Barrado y Navascués, D., Bouvier, J., & Stauffer, J. R. 2005, A&A, 436, 853
Looney, L. W., Mundy, L. G., & Welch, W. J. 2000, ApJ, 529, 477
Lombardi, M. & Alves, J. 2001, A&A, 377, 1023
Luhman, K. L., Rieke, G. H., Lada, C. J., & Lada, E. A. 1998, ApJ, 508, 347
Mardones, D., Myers, P. C., Tafalla, M., Wilner, D. J., Bachiller, R., & Garay, G. 1997, ApJ, 489, 719
Matthews, B. C., & Wilson, C. D. 2002, ApJ, 574, 822
Matthews, B. C., Hogerheijde, M. R., Jørgensen, J. K., & Bergin, E. A. 2006, ApJ, 652, 1374
McCaughrean, M. J., Rayner, J. T., & Zinnecker, H. 1994, ApJ, 436, L189
McCray, R. & Kafatos, M. 1987, ApJ, 317, 190
Miesch, M. S. & Bally, J. 1994, ApJ, 429, 645
Miesch, M. S., Scalo, J., & Bally, J. 1999, ApJ, 524, 895
Muench, A. A., Lada, C. J., Luhman, K. L., Muzerolle, J., & Young, E. 2007, AJ, 134, 411
Muench, A. A., Lada, E. A., Lada, C. J., Elston, R. J., Alves, J. F., et al. 2003, AJ, 125, 2029
Nakayama, M. 1988, M.S. thesis, Tohoku Univ.
O'Linger, J., Wolf-Chase, G., Barsony, M., & Ward-Thompson, D. 1999, ApJ, 515, 696
O'Linger, J. C., Cole, D. M., Ressler, M. E., & Wolf-Chase, G. 2006, AJ, 131, 2601
Olmi, L., Testi, L., & Sargent, A. I. 2005, A&A, 431, 253
Olano, C. A. & Poppel, W. G. L. 1987, A&A, 179, 202
Padoan, P. & Nordlund, Å. 1999, ApJ, 526, 279
Padoan, P., Boldyrev, S., Langer, W., & Nordlund, Å. 2003, ApJ, 583, 308
Padoan, P., Juvela, M., Goodman, A. A., & Nordlund, Å. 2001, ApJ, 553, 227
Padoan P., Bally J., Billawala, Y., Juvela, M., Nordlund Å. 1999, ApJ, 525, 318
Quillen, A. C., Thorndike, S. L., Cunningham, A., Frank, A., Gutermuth, R. A., et al. 2005, ApJ, 632, 941
Rebull, L. M., Stapelfeldt, K. R., Evans, N. J., II, Jørgensen, J. K., Harvey, P. M., et al. 2007, ApJS, 171, 447

Ridge, N. A., Schnee, S. L., Goodman, A. A., & Foster, J. B. 2006a, ApJ, 643, 932
Ridge, N. A., Di Francesco, J., Kirk, H., Li, D., Goodman, A. A., et al. 2006b, AJ, 131, 2921
Rodríguez, L. F., Anglada, G., & Curiel, S. 1999, ApJS, 125, 427
Rodríguez, L. F., Anglada, G., Torrelles, J. M., Mendoza-Torres, J. E., Haschick, A. D., & Ho, P. T. P. 2002, A&A, 389, 572
Rosolowsky, E. W., Pineda, J. E., Foster, J. B., Borkin, M. A., Kauffmann, J., et al. 2008, ApJS, 175, 509
Sancisi, R., Goss, W. M., Anderson, C., Johansson, L. E. B., & Winnberg, A. 1974, A&A, 35, 445
Sandell, G. & Knee, L. B. G. 2001, ApJ, 546, L49
Sargent, A. I. 1979, ApJ, 233, 163
Stauffer, J. R., Barrado y Navascues, D., Bouvier, J., Morrison, H. L., Harding, P., et al. 1999, ApJ, 527, 219
Steenbrugge, K. C., de Bruijne, J. H. J., Hoogerwerf, R., & de Zeeuw, P. T. 2003, A&A, 402, 587
Stenholm L.G. 1985, A&A, 144, 179
Strom, S. E., Strom, K. A., & Carrasco, L. 1974, PASP, 86, 798
Sun, K., Kramer, C., Ossenkopf, V., Bensch, F., Stutzki, J., & Miller, M. 2006, A&A, 451, 539
Tafalla, M., Bachiller, R., Martin-Pintado, J., & Wright, M.C.H. 1993, ApJ, 415, L139
Tsujimoto, M., Kobayashi, N., & Tsuboi, Y. 2005, AJ, 130, 2212
Ungerechts, H. & Thaddeus, P. 1987, ApJS, 63, 645
Walawender, J., Bally, J., Reipurth, B., & Aspin, C. 2004, AJ, 127, 2809
Walawender, J., Bally, J., & Reipurth, B. 2005a, AJ, 129, 2308
Walawender, J., Bally, J., Kirk, H., & Johnstone, D. 2005b, AJ, 130, 1795
Walawender, J., Bally, J., Kirk, H., Johnstone, D., Reipurth, B., & Aspin, C. 2006, AJ, 132, 467
Walawender, J., Reipurth, B., & Bally, J. 2008, AJ (submitted)
Watson, R. A., Rebolo, R., Rubiño-Martín, J. A., Hildebrandt, S., Gutiérrez, C. M., et al. 2005, ApJ, 624, L89
Wolf-Chase, G. A., Barsony, M., & O'Linger, J. 2000, AJ, 120, 1467
Wu, Y., Wei, Y., Zhao, M., Shi, Y., Yu, W., et al. 2004, A&A, 426, 503
Yamauchi, S., Tsuboi, Y., & Koyama, K. 2001, PASJ, 53, 885
Yan, J., Wang, H., Wang, M., Deng, L., Yang, J., & Chen, J. 1998, AJ, 116, 2438
Yu, K. C., Billawala, Y., & Bally, J. 1999, AJ, 118, 2940